Neuron

Article

TMEM63B functions as a mammalian hyperosmolar sensor for thirst

Highlights

- Hyperosmolarity can directly activate SFO excitatory neurons and this requires TMEM63B
- Heterologous expression of TMEM63B in culture cells responds to osmolarity change
- TMEM63B is a pore-forming subunit of the hyperosmosensitive channel
- TMEM63B is required for water intake of mice under osmotic and dehydrated thirst

Authors

Wenjie Zou, Siqi Deng, Xingyu Chen, ..., Jingxin Wang, Zhiyong Liu, Zhiqiang Yan

Correspondence

zqyan@cimrbj.ac.cn

In brief

Zou et al. showed that TMEM63B is required for thirst-driven water intake. TMEM63B is a pore-forming subunit of the hyperosmosensitive channel and mediates the hypertonic-induced currents in SFO thirst-initiation neurons, supporting TMEM63B as a mammalian hyperosmolar sensor for thirst.

Zou et al., 2025, Neuron *113*, 1–16
May 7, 2025
https://doi.org/10.1016/j.neuron.2025.02.012

CellPress

Please cite this article in press as: Zou et al., TMEM63B functions as a mammalian hyperosmolar sensor for thirst, Neuron (2025), https://doi.org/10.1016/j.neuron.2025.02.012

Neuron

CellPress

Article

TMEM63B functions as a mammalian hyperosmolar sensor for thirst

Wenjie Zou,[1,2,8] Siqi Deng,[2,3,8] Xingyu Chen,[2,4,8] Jiamin Ruan,[1,2,8] Huize Wang,[5] Wuqiang Zhan,[2] Jingxin Wang,[6,7] Zhiyong Liu,[6,7] and Zhiqiang Yan[1,2,5,9,*]

[1]Department of Neurobiology, School of Basic Medicine, Capital Medical University, Beijing, China
[2]Institute of Molecular Physiology, Shenzhen Bay Laboratory, Shenzhen, China
[3]Division of Life Science, The Hong Kong University of Science and Technology, Clear Water Bay, Hong Kong, China
[4]Department of Chemistry, Southern University of Science and Technology, Shenzhen, China
[5]Institute for Medical Physiology, Chinese Institutes for Medical Research, Beijing, China
[6]Institute of Neuroscience, State Key Laboratory of Neuroscience, CAS Center for Excellence in Brain Science and Intelligence Technology, Chinese Academy of Sciences, Shanghai, China
[7]University of Chinese Academy of Sciences, Beijing, China
[8]These authors contributed equally
[9]Lead contact
*Correspondence: zqyan@cimrbj.ac.cn
https://doi.org/10.1016/j.neuron.2025.02.012

SUMMARY

Thirst drives animals to reinstate water homeostasis by fluid intake. An increase in blood osmolality is thought to induce thirst by activating a hyperosmolar sensor expressed in the subfornical organ (SFO), but the molecular identity of this sensor remains elusive. Here, we provide behavioral and functional evidence to show that TMEM63B functions as a mammalian hyperosmolar sensor for thirst in SFO neurons. First, we showed that TMEM63B is expressed in SFO excitatory neurons and required for the neuronal responses to hypertonic stimulation. More importantly, heterologously expressed TMEM63B is activated by hypertonic stimuli, and point mutations can alter the reversal potential of the channel. Additionally, purified TMEM63B in liposomes exhibits osmolarity-gated currents. Finally, *Tmem63b* knockout mice have profound deficits in thirst, and deleting TMEM63B within SFO neurons recapitulated this phenotype. Taken together, these results provide a molecular basis for thirst and suggest that TMEM63B is a mammalian hyperosmolar sensor for thirst.

INTRODUCTION

Animals have the remarkable ability to sense their changing internal needs for water, and increased blood osmolality can trigger thirst.[1–5] Previously, the prevailing hypothesis was that thirst is primarily manifested as a sensation of dryness in the mouth and throat. However, our current comprehension demonstrates that thirst functions as a regulatory reaction to changes in the bloodstream. More precisely, thirst is triggered when there is a rise in plasma osmolality or a reduction in plasma volume or pressure.[6–10] Thirst acts as a driving force for animals to search for and consume water, effectively bringing these blood metrics back to their normal physiological levels. The advent of novel tools for recording and manipulating neural activity has yielded profound insights into the neural circuits in the subfornical organ (SFO), organum vasculosum of the lamina terminalis (OVLT), and the median preoptic nucleus (MnPO) that underlie thirst and drinking behavior.[11–21] Despite these advances, the specific molecular components (hyperosmolar sensor for thirst) that convert blood osmolarity into neural signals still remain an enigma.[4] Changes in blood osmolality can be detected in the SFO and OVLT in the forebrain.[22–29] These two sensory circumventricular organs' (CVOs) brain regions are located outside the blood-brain barrier and therefore have direct access to the circulation for plasma osmolarity sensing.[29] Specialized interoceptive neurons in the SFO and OVLT are intrinsically osmosensitive.[30–33] One hypothesis is that these SFO and OVLT interoceptive neurons monitor the blood osmolality directly through osmosensitive or mechanosensitive ion channels. To date, the identities of the ion channels responsible for osmosensing in SFO and OVLT interoceptive neurons remain elusive.[4] The utilization of optogenetic techniques to selectively activate SFO excitatory neurons has been demonstrated to elicit water-intake behavior in mice,[13] whereas the suppression of these SFO excitatory neurons abolished water consumption in thirst mice.[14] Furthermore, using *in vivo* calcium imaging, the peripheral administration of angiotensin or hypertonic saline has been shown to rapidly activate SFO excitatory neurons in a dose-dependent manner.[14] Collectively, these findings showed that SFO excitatory neurons are indispensable and sufficient in the initiation of thirst-related

Please cite this article in press as: Zou et al., TMEM63B functions as a mammalian hyperosmolar sensor for thirst, Neuron (2025), https://doi.org/10.1016/j.neuron.2025.02.012

behaviors. In the current study, we addressed whether SFO excitatory neurons are intrinsically hyperosmosensitive and what the underlying molecular mechanism is.

RESULTS

SFO excitatory neurons are intrinsically hyperosmosensitive

To examine whether SFO excitatory neurons can be directly activated by hypertonic stimuli, physiological recordings of these neurons under hypertonic stimulation were carried out. In the osmotic and dehydrated model of thirst, the plasma osmolality in mice was approximately 350 mOsm/kg[17,34,35]; our measurement further validated this, showing that the plasma osmolality in mice under osmotic thirst or water deprivation ranged from 360 to 370 mOsm/kg (Figure S1B). To establish the osmotic thirst model, mice were injected with 2 M NaCl intraperitoneally; to establish the water deprivation thirst model, mice were deprived of water for 48 h (Figure S1A). CaMK2α is a marker of excitatory neurons in the SFO.[13] We injected the rAAV2/9-CaMK2α-mCherry virus to label SFO excitatory neurons (Figure 1A). Action potentials (APs) were cell-attached recorded from SFO excitatory neurons labeled with red fluorescence under isotonic and hypertonic conditions (Figures 1B and S2A–S2C). SFO excitatory neurons from 5-week-old mice exhibited a pronounced increase in AP firing in response to the hypertonic stimulus of 315 and 350 mOsm/kg, which is within the range of the hyperosmolarity levels measured in the blood plasma of water deprivation or the osmotic thirst mice model (Figures 1B, S1A, and S1B).[17,34,35] To test whether the half-maximal effective concentration (EC50) of SFO excitatory neurons' hyperosmosensitivity falls within physiological range, we utilized a spectrum of hypertonic stimuli ranging from 315 to 390 mOsm/kg and observed a pronounced, dose-dependent response in SFO excitatory neurons (Figure 1C), with an EC50 of 347.7 mOsm/kg. This value lies within this physiological range of hyperosmolarity (Figure 1D), indicating that SFO excitatory neurons are highly sensitive to hypertonic stimuli and can be activated by the physiological plasma hyperosmolarity in thirst mice. In the range of hyperosmolarity we tested, 350 mOsm/kg is close to the plasma hyperosmolarity in two thirst models, whereas 315 mOsm/kg may represent a milder stimulus in moderate thirst. To validate that currents generated by the 315 mOsm/kg (about 12 pA) can still induce AP firing change, we injected 15 pA current in SFO excitatory neurons and found that it can induce robust 6 Hz AP firing (Figures S2D and S2E). Interestingly, SFO excitatory neurons showed higher membrane resistance (about 2 GΩ) compared with CA1 pyramidal neurons (less than 1 GΩ) (Figure S2F), one kind of well-studied excitatory neurons. This higher membrane resistance might enable SFO excitatory neurons to be more excitable to current inputs.

To further test whether SFO excitatory neurons are intrinsically hyperosmosensitive, we performed patch-clamp recording on the isolated SFO excitatory neurons, labeled by rAAV2/9-CaMK2α-mCherry virus. 2 to 3 days after the isolation and culture of the primary SFO neurons, current under −70 mV voltage-clamp was whole-cell recorded from excitatory neurons under an isotonic condition or hypertonic condition of 350 mOsm/kg (Figure S3A). With hyperosmotic stimulation, we observed an inward current of approximately 20 pA in isolated SFO excitatory neurons, consistent with the result displayed in *ex vivo* brain slices (Figures S3B and S3C). Taken together, these data indicated that hyperosmosensitivity is the intrinsic property of SFO excitatory neurons.

TMEM63B is required for the intrinsic hyperosmosensitivity of SFO excitatory neurons

Based on the hypothesis that SFO excitatory neurons directly monitor blood osmolality by osmosensitive or mechanosensitive ion channels, we analyzed the expression of known osmosensitive or mechanosensitive ion channels, including the Piezo1/2, transmembrane channel-like protein 1/2 (TMC1/2), and transmembrane protein 63 (TMEM63) family channels in these neurons,[36–53] using published single-cell sequencing data collected from the SFO.[17] We found that *Tmem63b* mRNA is enriched in SFO excitatory neurons (Figure S4). TMEM63B is a member of TMEM63/OSCA family of osmosensitive or mechanosensitive ion channels that are conserved from plants to animals.[39,40,54–65] The mammalian TMEM63 family has three members, TMEM63A, TMEM63B, and TMEM63C, and their osmosensing ability and physiological function in mammals are worthy of study.[42,66–74]

To analyze TMEM63B protein expression in the SFO, we generated a polyclonal antibody against mouse TMEM63B and found that TMEM63B is expressed in the SFO (Figure S5A). To further validate the endogenous expression of TMEM63B in the SFO, we used genetically edited $Tmem63b^{HA\text{-}fl/HA\text{-}fl}$ mice in which the tandem hemagglutinin (HA) and 3×FLAG tags were inserted after the N-terminal signal sequence in exon 2 of the *Tmem63b* gene and two locus of X-over of P1 (LoxP) sites were inserted into intron 1 and intron 4 of the *Tmem63b* gene.[42] Immunofluorescence staining against HA or FLAG revealed that TMEM63B is highly expressed in the SFO (Figures 2A, 2B, and S5B) but not in the OVLT and MnPO (Figures S5C and S5D). By immunostaining for CaMK2α and HA in $Tmem63b^{HA\text{-}fl/HA\text{-}fl}$ mice, we found that the majority of excitatory neurons (80.48% ± 1.50%) in the SFO express TMEM63B (Figure 2C).

Considering that TMEM63B expression may not correlate with SFO neurons' osmosensing capacity, we further tested whether TMEM63B in SFO excitatory neurons plays a functional role in sensing hyperosmolarity by injecting the rAAV2/9-CaMK2α-Cre-mCherry recombinant adeno-associated virus into the SFO of $Tmem63b^{HA\text{-}fl/HA\text{-}fl}$ mice to selectively knock out *Tmem63b* in SFO excitatory neurons. The spontaneous AP firing rate of SFO excitatory neurons from 5-week-old mice showed no significant difference between conditional knockout (cKO) and wild-type (WT) group (Figures S2B and S2C), and the basic intrinsic properties in SFO excitatory neurons also showed no significant difference, including resting membrane potential, AP threshold, AP rheobase, and membrane input resistance (Figure S6). TMEM63B-deficient SFO excitatory neurons have a typical response to glutamate puffing (Figures S7A and S7B) and angiotensin II (AngII) application, indicating that TMEM63B-deficient SFO excitatory neurons are generally healthy and have a normal response to non-osmolarity stimuli (Figures S7C–S7F). Under 315 mOsm/kg hyperosmolarity, the AP firing rate of WT SFO excitatory neurons rises from 0.69 to 2.4 Hz upon stimulation; under 350 mOsm/kg, the firing rate undergoes a more dramatic change from 0.78 to 4.34 Hz, but these

Please cite this article in press as: Zou et al., TMEM63B functions as a mammalian hyperosmolar sensor for thirst, Neuron (2025), https://doi.org/10.1016/j.neuron.2025.02.012

CellPress

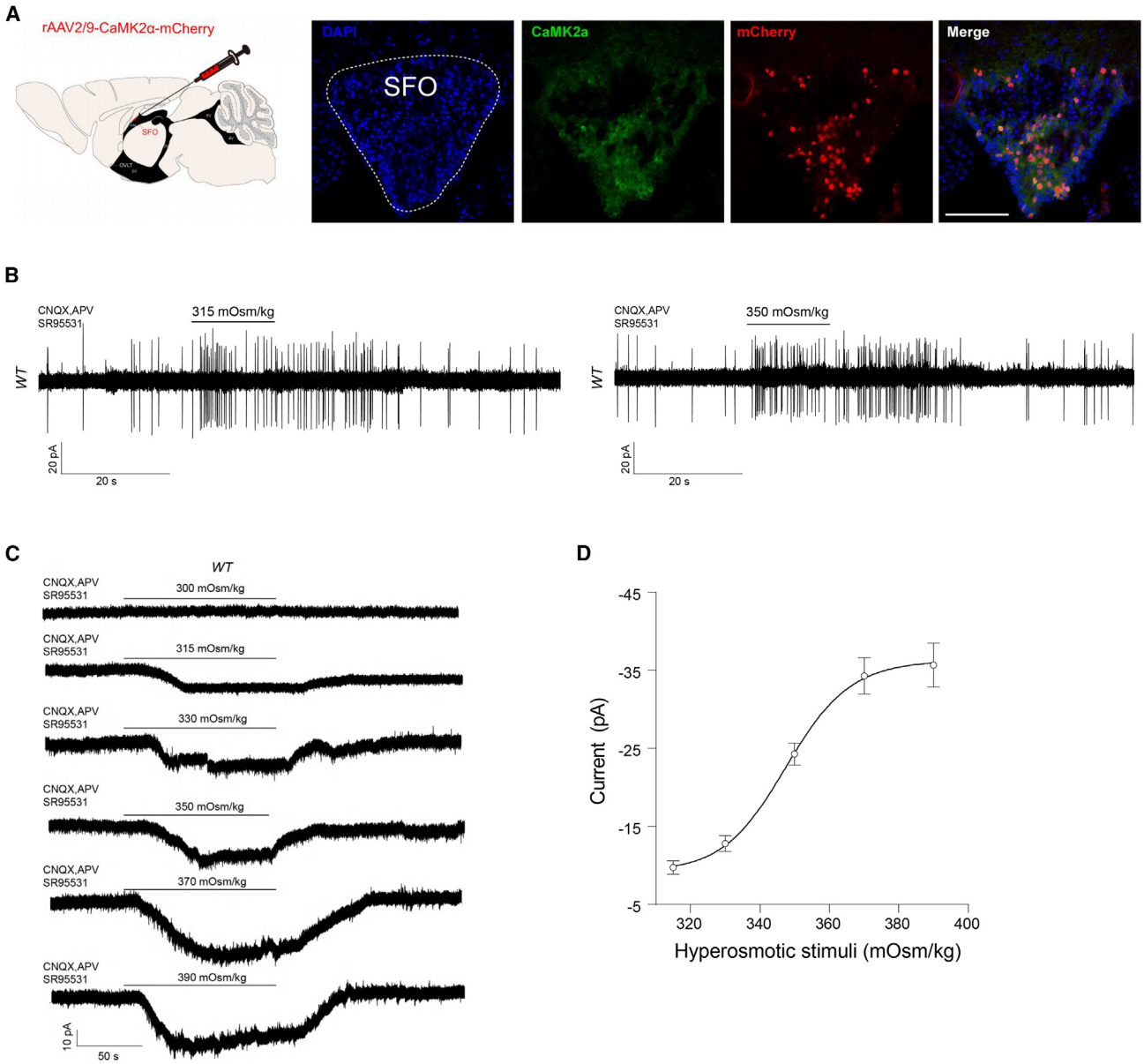

Figure 1. SFO excitatory neurons respond to hyperosmolarity changes with AP firing and inward excitatory currents

(A) Left, schematic diagram of labeling SFO excitatory neurons by injecting AAV-CaMK2α-mCherry in the SFO. Right, representative images show mCherry expression in SFO excitatory neurons. Scale bar, 100 μm; mCherry (red) was expressed under the CaMK2α promoter. Green indicates endogenous CaMK2α, which labels excitatory neurons.

(B) Representative traces of action potential (AP) firing of SFO excitatory neurons in 5-week-old wild-type (WT) mice. The basal AP firing rate of SFO excitatory neurons was first recorded in isotonic stimuli (300 mOsm/kg) for more than 20 s and the neurons were exposed to a brief 15-s puff of hypertonic solution at 315 or 350 mOsm/kg. The firing of SFO excitatory neurons in WT mice shows a reversible increase in response to the hypertonic stimulus.

(C) Representative traces of current recorded in SFO excitatory neurons in response to isotonic and hypertonic stimuli ranging from 315 to 390 mOsm/kg. After recording in isotonic solution for 1 min, hypertonic perfusion was applied to SFO excitatory neurons for 2 min, followed by an isotonic washout.

(D) The hyperosmolarity-induced currents at −70 mV in SFO excitatory neurons increased with the gradient of evaluated hyperosmotic stimulus, with its EC50 as 347.7 mOsm/kg (n = 4–6 for each hyperosmotic stimulation level, n represents the number of SFO excitatory neurons).

increases were not observed in TMEM63B-deficient neurons (Figures 2D and 2F). The hyperosmolarity-sensitive current was also lost in TMEM63B-deficient SFO excitatory neurons (Figures 2E and 2G). Similarly, in isolated TMEM63B-deficient SFO excitatory neurons, hypertonic stimuli also failed to elicit a significant response (Figures S3B and S3C). We also performed recording on brain slices from older mice aged 12 weeks old. The robust increase in AP firing rate in SFO excitatory neurons induced by hyperosmolarity was absent in *Tmem63b* cKO mice, similar to the observation in 5-week-old mice

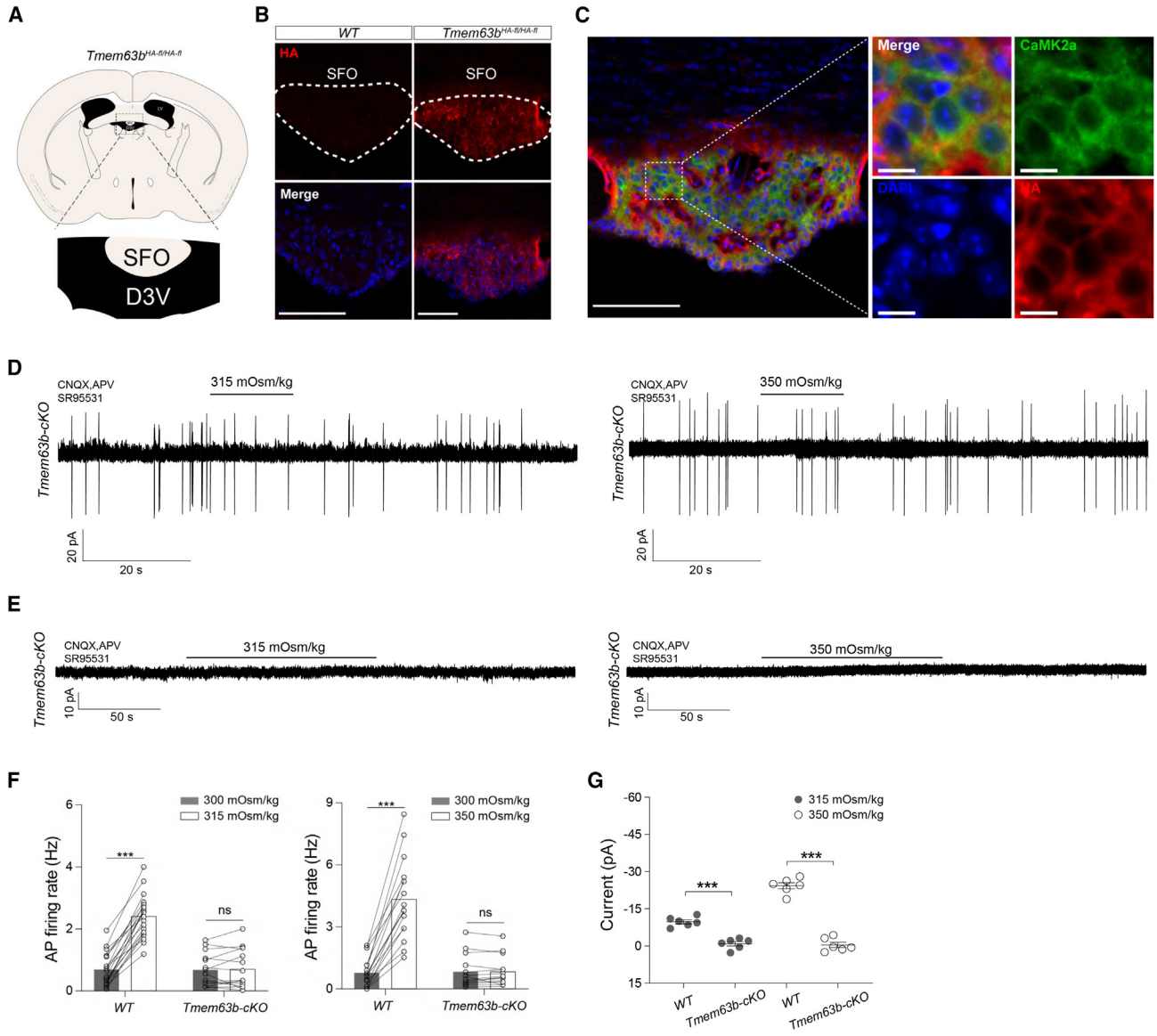

Figure 2. TMEM63B is required for the activation of SFO excitatory neurons in response to osmolarity changes

(A) The schematic diagram shows the anatomical location of the SFO (coronal view). D3V, dorsal third ventricle.

(B) Endogenous TMEM63B is expressed in the SFO. TMEM63B is labeled by a fusion HA tag in *Tmem63b*$^{HA\text{-}fl/HA\text{-}fl}$ mice. Red indicates immunofluorescence staining against HA, showing that TMEM63B is expressed in the SFO. Blue indicates nuclear staining. WT, wild type. Scale bar, 100 μm.

(C) TMEM63B labeled by a fusion HA tag (red) is highly expressed in CaMK2α-positive (green) excitatory neurons. Scale bar: left, 100 μm; right, 20 μm.

(D) Representative traces of action potential (AP) firing of SFO excitatory neurons in 5-week-old *Tmem63b* cKO mice. No significant difference in AP firing rate was observed upon hyperosmotic stimuli of 315 or 350 mOsm/kg.

(E) Representative traces of current recorded in TMEM63B-deficient SFO excitatory neurons in response to hypertonic stimuli of 315 or 350 mOsm/kg, showing no significant response in both conditions.

(F) The AP firing of SFO excitatory neurons in response to hypertonic stimuli is dramatically reduced in 5-week-old *Tmem63b* cKO mice (n = 14–20). n represents the number of SFO excitatory neurons.

(G) Hyperosmosensitive currents induced by 315 mOsm/kg (left) or 350 mOsm/kg (right) were eliminated in TMEM63B-deficient SFO excitatory neurons (n = 6). n represents the number of SFO excitatory neurons.

All error bars denote the mean ± SEM, n.s., non-significant difference, ***p < 0.001, **p < 0.01, Student's unpaired t test.

(Figures S8A, S8B, and S8E). The spontaneous firing rate of *Tmem63b* cKO SFO excitatory neurons from 12-week-old mice showed a mild decrease compared with the control in isotonic solution (Figures S8A, S8B, and S8E). This decreased basal firing rate of *Tmem63b* KO SFO excitatory neurons was also reported by a recently published paper,[73] and its underlying mechanism requires further investigation. The hyperosmosensitive current that occurred in the control group was lost in

Please cite this article in press as: Zou et al., TMEM63B functions as a mammalian hyperosmolar sensor for thirst, Neuron (2025), https://doi.org/10.1016/j.neuron.2025.02.012

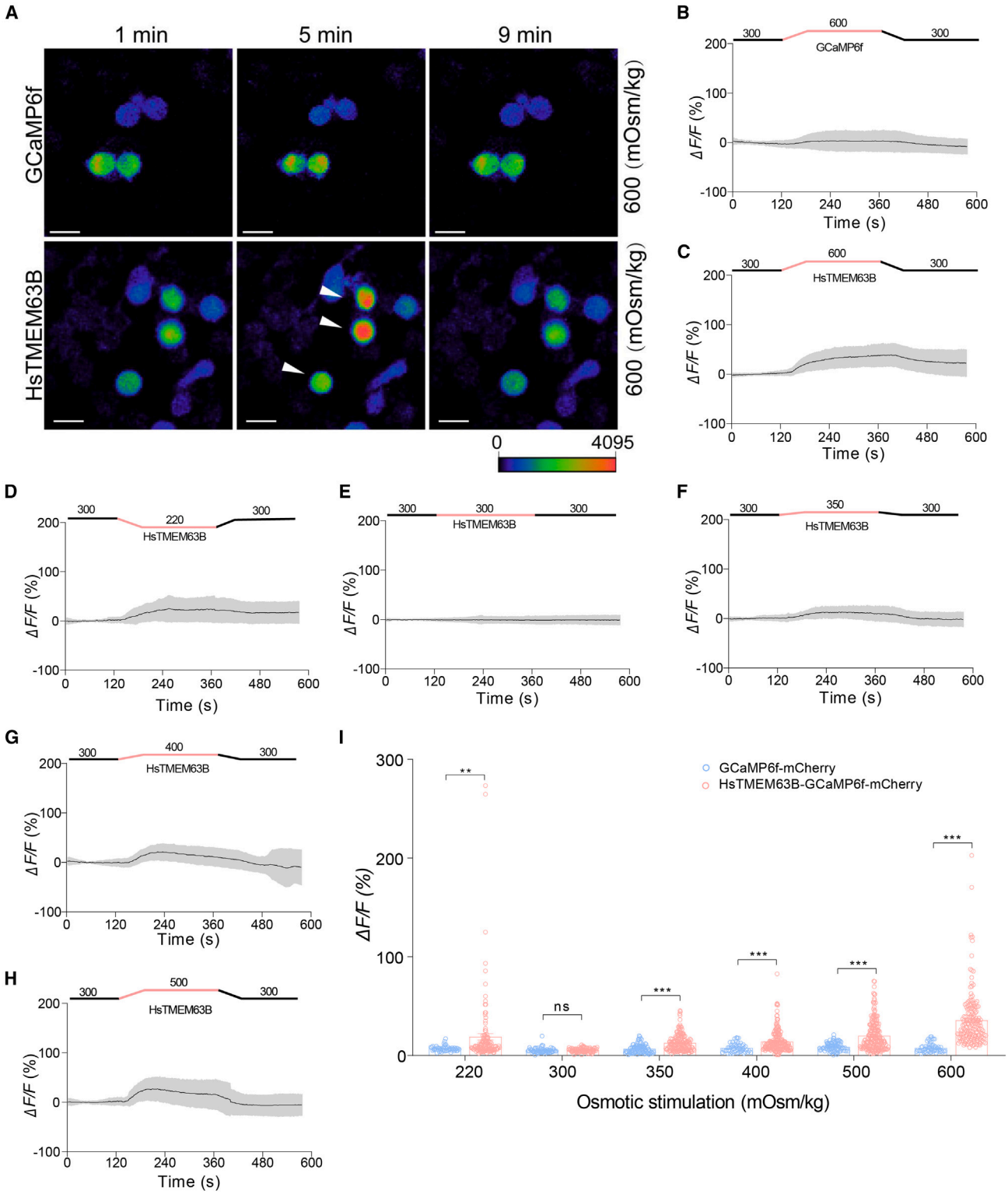

Figure 3. Heterologously expressed TMEM63B mediates calcium influx in response to hypertonic stimulus

(A) Representative images show calcium signaling responses in N2a cells under 600 mOsm/kg hyperosmotic stimuli, with heterologous expression of pCMV6-GCaMP6f-IRES-mCherry or pCMV6-HsTMEM63B-P2A-GCaMP6f-IRES-mCherry. Arrowhead marks cells with cytosolic calcium increase. Scale bar, 20 μm.

(legend continued on next page)

Please cite this article in press as: Zou et al., TMEM63B functions as a mammalian hyperosmolar sensor for thirst, Neuron (2025), https://doi.org/10.1016/j.neuron.2025.02.012

TMEM63B-deficient SFO excitatory neurons (Figures S8C, S8D, and S8F). In summary, these results indicate that TMEM63B is required for osmotic sensing of excitatory neurons in the SFO.

Heterologously expressed TMEM63B in cultured cells responds to osmolarity changes

If TMEM63B is the primary sensor that mediates thirst in SFO excitatory neurons, it should be activated directly by hypertonic stimulation. To test this hypothesis, we examined whether heterologously expressed TMEM63B could form osmosensitive channels in culture cells. We first co-expressed human TMEM63B (HsTMEM63B) and GCaMP6f in N2a cells and monitored the fluorescence intensity of transfected N2a cells during hypertonic stimulation. We stimulated the cells by changing the bath solution from an isotonic condition to a gradient of hyperosmotic solutions (350–600 mOsm/kg). Compared with cells transfected with GCaMP6f alone (Figures S9A–S9E), TMEM63B-expressing cells exhibited a significant calcium response under hyperosmolarity. Notably, the calcium fluorescence intensity in TMEM63B-expressing cells increased gradually with the increasing hyperosmolarity (Figures 3A–3C and 3E–3I). The calcium signals of TMEM63B-expressing cells coincided with the osmolarity changes during solution perfusion (Figure S9F). We also tested a hypoosmolarity of 220 mOsm/kg and found that it induced a calcium influx at a similar extent to that in 600 mOsm/kg hyperosmolarity (Figures 3D and 3I). These results show that heterologous expression of TMEM63B in N2a cells responds to a range of osmotic stimuli, indicating that TMEM63B has a unique feature that enables it to respond to osmolality changes.

To further validate that TMEM63B is an osmolarity-sensing ion channel, we recorded osmolarity-activated currents in Chinese hamster ovary (CHO) cells transfected with HsTMEM63B with hypertonic stimulus by patch-clamp recording. The cells were recorded in isotonic solution (300 mOsm/kg) for 2 min and then a gradient of hypertonic solutions, ranging from 320 to 600 mOsm/kg, was applied for 3 min, respectively, before isotonic washout. To examine the hypertonic current responses at different voltages, a ramp protocol (−80 to +80 mV) was applied every 2 s. CHO cells transfected with HsTMEM63B showed hyperosmolarity-induced currents (Figures 4A–4D), and the currents at −70 mV in the ramp protocol were plotted over time (Figures 4A and 4C). The magnitude of the hyperosmolarity-sensitive current in TMEM63B-overexpressing cells increased with the degree of stimulation (Figures 4G–4L). Hyperosmotic stimuli at 320 and 350 mOsm/kg, resembling the blood osmolality in osmotic or dehydrated animal models, were able to induce osmosensitive currents in TMEM63B-expressing CHO cells (Figures 4H, 4I, and 4L); stronger hyperosmolarity of 400, 500, and 600 mOsm/kg induced larger currents in CHO cells expressing TMEM63B (Figures 4C and 4J–4L). In contrast, the control cells without *TMEM63B* transfection showed no hyperosmosensitive current (Figure S10). Additionally, the hyperosmotic-sensitive current under 500 mOsm/kg solution in TMEM63B-expressing CHO cells can be largely blocked by 100 μM ruthenium red (Figures 4E and 4F). These results suggest that TMEM63B can mediate osmolarity-induced current and is likely to be an osmolarity-sensing ion channel.

TMEM63B is likely a pore-forming subunit of a hyperosmosensitive channel

Although N2a and CHO cells heterogeneously expressing HsTMEM63B exhibit strong sensitivity to hyperosmotic stimulus, whether TMEM63B is a pore-forming subunit of the osmosensitive channel remains unknown. To answer this question, we first built two homologous structures of HsTMEM63B by SWISS-MODEL and AlphaFold and mapped a putative pore region in the predicted structures (Figure 5A), based on previously published structures of the plant OSCA/TMEM63 channels. By analyzing the structure and alignment of the multiple homologous members of TMEM63B (Figure S11), we identified a conserved glutamic acid residue (E510) in the putative pore region, which is negatively charged and may contribute to the cation selectivity of TMEM63B (Figure 5B). Then, we generated alanine and lysine substitution at this site, E510A and E510K, respectively, and expressed them in CHO cells to record hyperosmolarity-induced currents. To analyze the effects of these two mutations, we recorded the whole-cell currents and switched the bath solution from an isotonic solution (300 mOsm/kg) to a hyperosmotic solution (500 mOsm/kg). The currents at −70 mV were plotted to show the electrophysiological response of *TMEM63B*-transfected cells to the osmolarity change (Figures 5C and 5D). E510A showed a clear response to hypertonic stimulus, whereas the current response was barely detectable in the E510K mutant (Figures 5C and 5D). E510A also shifted the reversal potential of the current induced by a hypertonic stimulus (Figures 5D and 5E), suggesting that TMEM63B is likely a pore-forming subunit of an osmolarity-sensing channel.

To test whether purified TMEM63B proteins were sufficient to recapitulate the channel properties recorded from CHO cells transfected with *TMEM63B*, we reconstituted the purified MmTMEM63B proteins into liposomes (Figure 5F). The purified MmTMEM63B-3FLAG-eGFP (127.8 kDa) migrated as smeared bands on sodium dodecyl sulphate-polyacrylamide gel electrophoresis (SDS-PAGE) (Figure 5G). Our previous study shows

(B and C) The calcium fluorescence intensity in response to the hypertonic solution (600 mOsm/kg). N2a cells were heterologously transfected with pCMV6-GCaMP6f-IRES-mCherry or pCMV6-HsTMEM63B-P2A-GCaMP6f-IRES-mCherry. The red line indicates the hyperosmotic stimulus for 4 min (n = 82–135, n represents the number of N2A cells).

(D–H) The calcium fluorescence intensity of N2a cells heterologously expressing pCMV6-TMEM63B-P2A-GCaMP6f-IRES-mCherry in response to hypoosmolarity of 220 mOsm/kg (D), isotonic solution (E), and hyperosmolarity of 350 mOsm/kg (F), 400 mOsm/kg (G), and 500 mOsm/kg (H) (n = 49–143, n represents the number of N2A cells in each hypoosmotic and hyperosmotic stimulation level).

(I) Quantification of the calcium response in TMEM63B-expressing N2a cells in response to a range of osmotic stimulations, presented as an increase in fluorescence intensity after osmotic stimulation (ΔF) relative to that before stimulation (F_0) (n = 52–199, n represents the number of N2A cells in each hypoosmotic and hyperosmotic stimulation level). As the degree of hyperosmolarity increased, TMEM63B-expressing N2a cells showed increased calcium signals.

The gray shadow in the calcium imaging trace for (B)–(H) denotes the mean ± SD. Error bars for (I) denote the mean ± SEM; n.s., non-significant difference, ***$p < 0.001$; Student's unpaired t test.

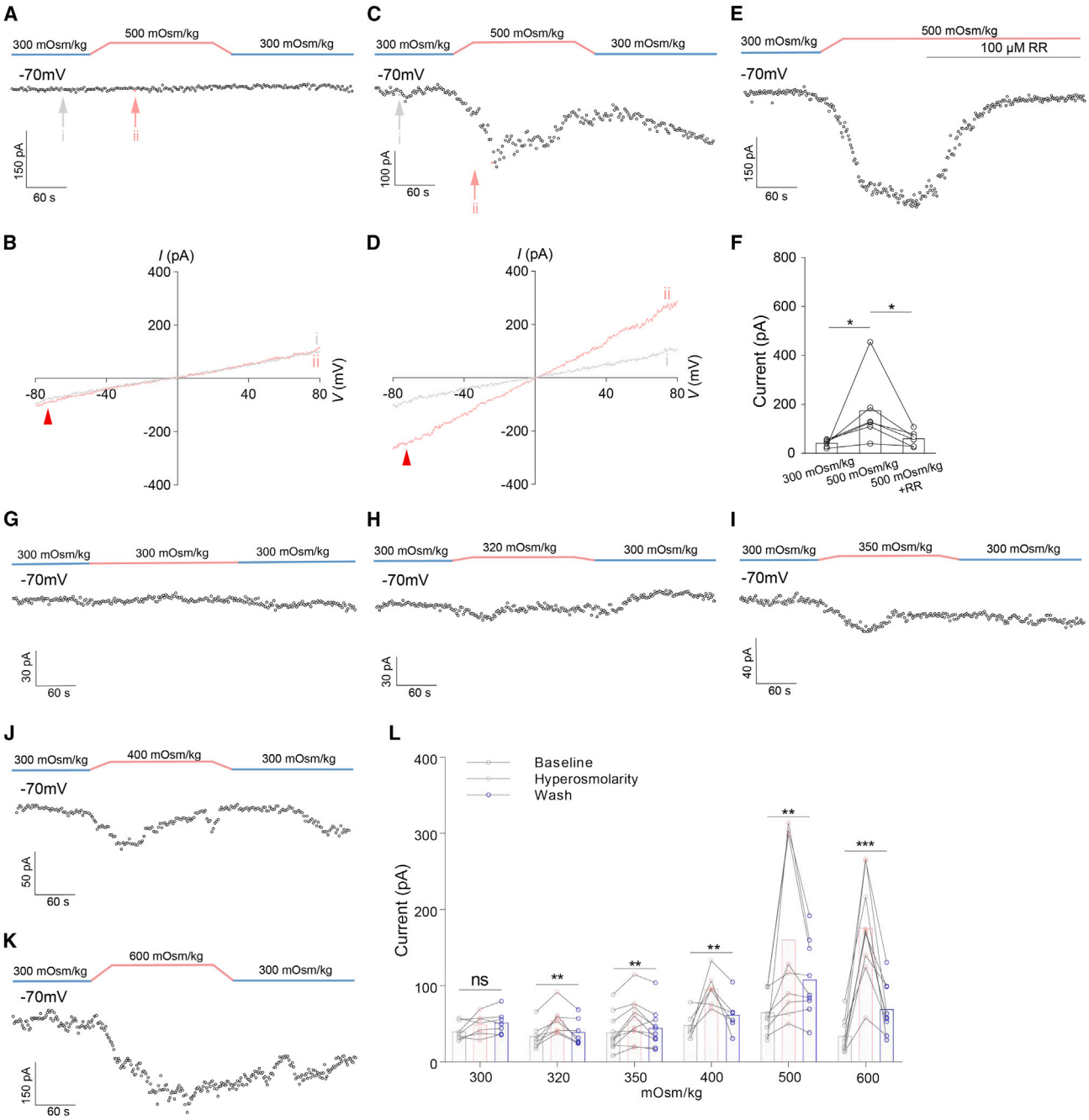

Figure 4. Heterologously expressed TMEM63B mediates hyperosmosensitive currents

(A and B) Representative whole-cell currents in untransfected CHO cells were recorded every 2 s by ramp protocols in 2-min isotonic solution (300 mOsm/kg; blue) and 3-min hyperosmotic solution (500 mOsm/kg; red) before isotonic washout. *I-V* curves at times indicated during hypertonic stress (red arrow in A) and isotonic solution (gray arrow in A) are shown in (B). Currents at −70 mV (arrowhead in B) over time were plotted in (A).

(C and D) Representative whole-cell currents in CHO cells transfected with HsTMEM63B-eGFP were recorded in 2-min isotonic solution (300 mOsm/kg; blue) and 3-min hyperosmotic solution (500 mOsm/kg; red) before isotonic washout. *I-V* curves at times indicated during hypertonic stress (red arrow in C) and isotonic solution (gray arrow in C) are shown in (D). Currents at −70 mV (arrowhead in D) over time were plotted in (C).

(E) Representative whole-cell currents in CHO cells transfected with HsTMEM63B-eGFP were recorded in 2-min isotonic solution (300 mOsm/kg; blue) and 3-min hyperosmotic solution (500 mOsm/kg; red) with the application of ruthenium red (RR). Currents at −70 mV over time were plotted.

(F) The current induced by hyperosmolarity in TMEM63B-expressing CHO cells can be largely blocked by RR (n = 6).

(legend continued on next page)

Please cite this article in press as: Zou et al., TMEM63B functions as a mammalian hyperosmolar sensor for thirst, Neuron (2025), https://doi.org/10.1016/j.neuron.2025.02.012

that the *At*OSCA1.1 protein, a homologous protein of TMEM63B in plants, was glycosylated when expressed in HEK293F cells.[56] To test whether mouse TMEM63B was also glycosylated when expressed in HEK293F cells, we treated the purified MmTMEM63B-3FLAG-eGFP with a protein deglycosylation mixture; the treatment notably diminished the smear in the bands (Figure 5G). Mass spectrometry examination of the purified MmTMEM63B-eGFP identified three N-glycosylated amino acid sites (Figure S12). These results indicated that the smeared bands in SDS-PAGE were due to glycosylation rather than other proteins. Next, we incorporated MmTMEM63B into liposomes for patch-clamp recordings[43] and eGFP-tagged MmTMEM63B localized in the liposome membrane (Figure 5H).

The currents were recorded in the patches excised from empty liposomes and liposomes reconstituted with MmTMEM63B in the isotonic or hypertonic application ranging from 320 to 600 mOsm/kg. We found that, with a gradient of elevated hyperosmolarity ranging from 320 to 600 mOsm/kg, an increasing integrated current of TMEM63B in liposomes was recorded (Figures 5I and 5K). The hyperosmolarity-induced currents in the TMEM63B-reconstituted liposomes under 500 mOsm/kg were eliminated by 30 μM $GdCl_3$ (Figures 5I and 5J). As further negative controls, empty liposomes or liposomes constituted with heat-denatured TMEM63B also failed to produce channel activity under hyperosmolarity stimulus (Figures 5I and 5J). These results suggested that TMEM63B is likely a pore-forming subunit of a hyperosmosensitive channel.

TMEM63B is required for the drinking behavior of mice in the osmotic thirst and dehydrated thirst model

Having found that TMEM63B is an osmolarity-sensitive channel and identified the functional role of TMEM63B in SFO excitatory neurons' activation by hypertonic stimuli in brain slices, we tested whether TMEM63B is required for the activation of SFO excitatory neurons in thirst models *in vivo*. After osmotic thirst or dehydrated thirst modeling (Figure S1A), control and *Tmem63b* KO mice were sacrificed for immunostaining using c-Fos as a marker of thirst-evoked neuronal activity within the SFO. Consistent with previous studies,[13,17] we found that SFO excitatory neurons are robustly activated, as indicated by c-Fos expression under osmotic thirst or dehydrated thirst, and this activation was greatly reduced in *Tmem63b* KO mice (Figures 6A–6F). These results indicate that TMEM63B is required for SFO excitatory neuron activation in thirst.

Having found that TMEM63B is required for the activation of SFO excitatory neurons during thirst stress and that TMEM63B is a pore-forming ion channel to detect osmolarity changes, to finally determine whether TMEM63B is the mammalian hyperosmolar sensor for thirst, we investigated whether TMEM63B plays a role in mediating thirst behavior in mice. First, we analyzed the drinking behaviors of water-sated mice to determine the water intake without modeling; no significant differences were found in water intake between water-sated *Tmem63b* KO and control mice during a 1-h test (Figures 7C and 7D). Then, we examined the drinking behavior of *Tmem63b* KO mice in the osmotic thirst model and dehydrated thirst model. Employing a two-choice consumption preference assay,[1,11,17,20] mice in the osmotic thirst model or dehydrated thirst model were tested for the preference between water and 0.3 M NaCl (Figure 7A). Consistent with previous studies,[1,11,17,20] acute osmotic stress with hypertonic solution induced selective consumption of water over the 0.3-M NaCl solution (Figure S13A). Moreover, the number of licks and the drinking volume of water of *Tmem63b* KO mice were greatly reduced compared with those of WT mice under the osmotic thirst model (Figure 7C). A similar phenotype of *Tmem63b* KO mice was found in the water deprivation model (Figures 7D and S13B), indicating that TMEM63B is required for both osmotic and dehydrated thirst. Notably, the water intake in *Tmem63b* KO mice under both types of thirst was still larger than that in water-sated control mice (Figures 7C and 7D), which was around 0.1 mL within 1 h, suggesting that other mechanisms may also be involved in osmotic and water deprivation thirst.

To determine the role of TMEM63B in SFO excitatory neurons in thirst behavior, we injected the rAAV2/9-CaMK2α-Cre-mCherry virus into the SFO of *Tmem63b*$^{HA\text{-}fl/HA\text{-}fl}$ mice to selectively KO *Tmem63b* in SFO excitatory neurons (Figure 7B). No significant differences in drinking behavior were observed between control and *Tmem63b* cKO mice under a water-sated state during a 1-h test (Figures 7E and 7F). Similar to the global *Tmem63b* KO model, in both the osmotic thirst model and dehydrated thirst model, *Tmem63b-cKO* mice consumed much less water than WT mice (Figures 7E, 7F, S13C, and S13D), demonstrating that TMEM63B deficiency specifically in SFO excitatory neurons impairs thirst in mice. Within this set of experiments, the water intake in water-sated WT mice was still lower than that in *Tmem63b* cKO mice, implying that alternative pathways might concurrently contribute to the thirst response elicited by osmotic changes and water deprivation (Figures 7E and 7F).

To further explore the function of TMEM63B as a hyperosmolar sensor for thirst, we examined whether overexpression of TMEM63B leads to an increase in thirst phenotypes. We employed a model of moderate thirst, which might provide a more sensitive readout of its function. To be specific, we used 1 M NaCl instead of 2 M NaCl for the osmotic thirst model and 36 h water deprivation instead of 48 h for the dehydration model. We first measured the plasma osmolarity to ensure a successful generation of thirst models in different extents, in which the plasma osmolarity of mice with a 1-M NaCl injection (354 mOsm/kg) and 36 h water deprivation (343 mOsm/kg) was lower than that with a 2-M NaCl injection and 48 h water deprivation (360–370 mOsm/kg), respectively (Figure S14A). In both moderate thirst models, we observed significantly increased water intake or licking behavior in mice with TMEM63B overexpressed in SFO excitatory neurons (Figures S14B–S14E), supporting TMEM63B's role in thirst transduction.

(G–K) Representative whole-cell currents in CHO cells transfected with HsTMEM63B-eGFP in response to isotonic solution (G) and hyperosmolarity of 320 (H), 350 (I), 400 (J), and 600 mOsm/kg (K).

(L) The hyperosmolarity-induced currents at −70 mV in CHO cells expressing HsTMEM63B-eGFP increased with a gradient of evaluated hyperosmotic stimuli (320, 350, 400, 500, and 600 mOsm/kg, n = 6–10).

For (F) and (L), n presents the number of CHO cells. n.s., non-significant difference, $^{*}p < 0.05$, $^{**}p < 0.01$, $^{***}p < 0.001$; one-way ANOVA.

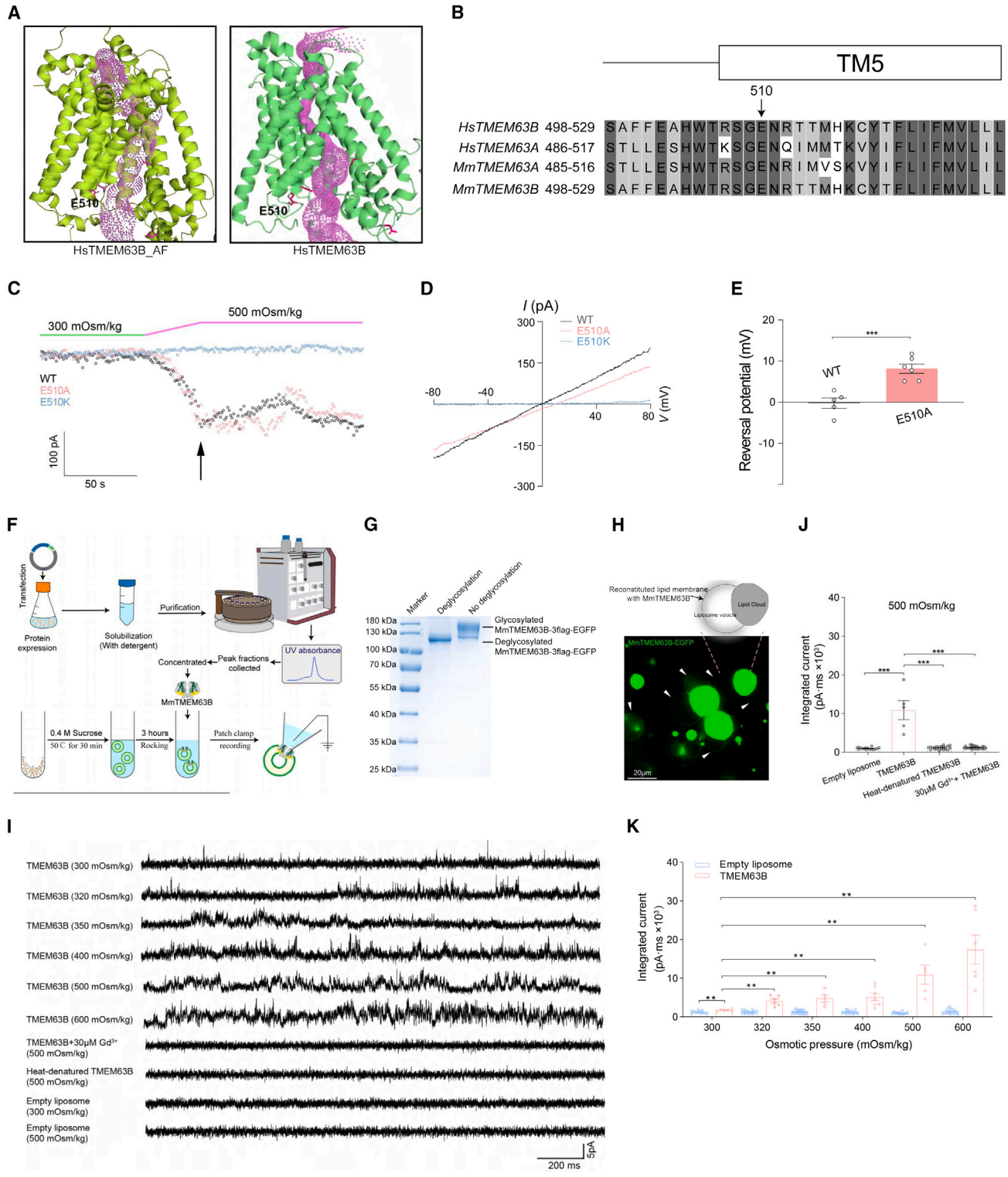

Figure 5. TMEM63B is likely a pore-forming subunit of a hyperosmosensitive channel

(A) A side view of the human TMEM63B transmembrane domain was obtained from an AlphaFold model (left) or a homology model based on OSCA 1.2 (PDB: 6ijz, right). The calculated pore profile of the putative HsTMEM63B is indicated as purple dots.

(B) Sequence alignment of human TMEM63B and its homologs. The arrow marks the negatively charged E510 residues in the putative pore region targeted for mutagenesis. Mm, *Mus musculus*; Hs, *Homo sapiens*.

(legend continued on next page)

Please cite this article in press as: Zou et al., TMEM63B functions as a mammalian hyperosmolar sensor for thirst, Neuron (2025), https://doi.org/10.1016/j.neuron.2025.02.012

In summary, the impairment in thirst behavior after *Tmem63b* KO and the enhancement of water consumption after TMEM63B overexpression in SFO excitatory neurons together provide compelling evidence that TMEM63B in SFO excitatory neurons is required for the water intake behavior of mice in the osmotic thirst and dehydrated thirst model.

DISCUSSION

Most mammals maintain a body fluid osmolality within a narrow range of approximately 300 mOsm/kg.[75] Under the osmotic or water deprivation model of thirst, the plasma osmolality in mice is approximately 350 mOsm/kg.[17,32,33] When body fluid osmolality increases, the animals feel thirsty and instinctively seek and consume water, restoring their body fluid osmotic pressure and plasma volume within the homeostatic range. The advent of novel techniques for neural recording and manipulation has yielded remarkable discoveries concerning the neural circuits involved in thirst and drinking behavior.[11–19,76–79] However, in contrast, the molecular identities of the primary hyperosmolar sensor for thirst, responsible for converting changes in blood osmolarity into neural signals, remain unknown.[4]

For a channel to be considered a bona fide transducer in SFO excitatory neurons of blood osmolality to thirst (hyperosmolar sensor for thirst), it should meet several criteria.[80] TMEM63B satisfies all of these criteria. First, it is expressed in SFO excitatory neurons that are critical for thirst; second, it is required for hypertonic-solution-induced excitation of SFO excitatory neurons; third, heterologous expression of TMEM63B in cultured cells generates osmolarity-sensitive channels; and fourth, purified TMEM63B shows hypertonic-induced currents. These results suggest that TMEM63B is a hyperosmolar sensor for thirst in mammals. Thirst is critical for water homeostasis and conceivably, a deficiency of TMEM63B might result in a deficit in water homeostasis and lead to hypertension or kidney diseases.

The OSCA/TMEM63 family is recognized as a family of ion channels that are sensitive to osmotic pressure and mechanical stimuli. Previous research has indicated that OSCAs in plants are hyperosmotic-sensitive ion channels,[54,55,57,58] whereas a later study showed that the TMEM63 family in mammals is hypoosmotic-sensitive instead of hyperosmosensitive,[42] suggesting that the hyperosmotic sensitivity of the OSCA/TMEM63 family may not be evolutionarily conserved. Our study demonstrates that TMEM63B is also a hyperosmotic-sensitive ion channel, indicating that the hyperosmotic sensitivity of the OSCA/TMEM63 family is conserved throughout evolution. However, the hypoosmotic sensitivity of TMEM63B appears to conflict with its role as a hyperosmolar sensor for thirst-mediating hyperosmotic excitation in SFO excitatory neurons in mammals. Accordingly, we tested the response of SFO excitatory neurons to hypotonic stimulation and found an outward current that contributed to an overall inhibitory effect on neuronal activity (Figures S15A and S15B), consistent with a previous finding.[33] We hypothesized that other channels in SFO neurons might contribute to this outward current. Analyzing single-cell sequencing data (Figure S4), we found that TWIK-related K^+ channel 1 (TREK1), a known hypoosmosensitive two-pore potassium channel,[81,82] is expressed in most SFO excitatory neurons. Our electrophysiology experiments in a heterologous system further confirmed the hypoosmosensitivity of TREK1 (Figures S15C and S15D); its activation in SFO excitatory neurons under hypotonic conditions might possibly lead to an outward current, overwhelming the effect of TMEM63B.

Although the sensing of force in the plasma membrane has been extensively investigated, the mechanisms and physiological functions of mechanotransduction in organelles are only starting to be revealed. Apart from the osmosensing and mechanosensitive functions on the plasma membrane, recent studies have revealed that TMEM63s in lysosomes modulate lysosomal morphology and function in N2A cells, and loss of DmTMEM63 function causes impaired lysosomal degradation, synaptic loss, progressive motor

(C) Representative currents at −70 mV over time induced by a 3-min 500 mOsm/kg hyperosmolarity stimulus were plotted for CHO cells transfected with wild type (WT) or the two putative selectivity filter mutants (E510A and E510K) of HsTMEM63B. Whole-cell currents were monitored every 2 s by ramp protocols from −80 to 80 mV for 100 ms.

(D) The E510A mutation altered the *I-V* curve of hyperosmolarity-induced currents, whereas the E510K mutation largely eliminated the osmosensitive current under hypertonic stimulus. *n* represents the number of cells. $n = 5$ for WT group, $n = 6$ for E510A group, $n = 4$ for E510K group.

(E) The E510A mutation shifted the reversal potential of TMEM63B currents activated by a hypertonic stimulus. Error bars denote the mean ± SEM, $^{***}p < 0.001$, Student's unpaired t test, $n = 5–6$. *n* represents the number of cells.

(F) Schematic diagram of size-exclusion chromatography (SEC) for MmTMEM63B protein purification and proteoliposome reconstitution procedure with the sucrose method for patch-clamp recording.

(G) SDS-PAGE analysis of purified MmTMEM63B proteins with an eGFP tag stained with Coomassie blue. The deglycosylation treatment resulted in a significant reduction in the band smearing observed in SDS-PAGE.

(H) Representative images show eGFP-labeled MmTMEM63B incorporated into liposome membranes (bottom) and a cartoon illustration (top). The white arrows indicate membranes with eGFP-labeled MmTMEM63B. Scale bar, 20 μm.

(I) Representative currents of MmTMEM63B incorporated into liposome membranes in response to isotonic solution or a gradient of hypertonic solutions. No current was recorded in the empty liposomes, MmTMEM63B-reconstituted liposomes with 30 μM $GdCl_3$, or proteoliposomes of heat-denatured MmTMEM63B in 500 mOsm/kg hyperosmotic solutions. All recordings were performed under +40 mV.

(J) Quantification of integrated current responses in empty liposomes, MmTMEM63B-reconstituted proteoliposomes with or without 30 μM $GdCl_3$, and the proteoliposome of heat-denatured MmTMEM63B in 500 mOsm/kg hyperosmotic solution holding at +40 mV. The area under the curve indicates the integrated currents ($n = 5–25$, *n* represents the number of proteoliposome recordings).

(K) Quantification of integrated current responses in empty liposomes and MmTMEM63B-reconstituted proteoliposomes under isotonic condition or a gradient of hypertonic conditions holding at +40 mV ($n = 5–22$, *n* represents the number of proteoliposome recordings).

$^{**}p < 0.01$, $^{***}p < 0.001$, Student's unpaired t test. All error bars denote the mean ± SEM. The response to 500 mOsm/kg of empty liposomes and MmTMEM63B-reconstituted liposomes in (J) and (K) were from the same group of data.

Please cite this article in press as: Zou et al., TMEM63B functions as a mammalian hyperosmolar sensor for thirst, Neuron (2025), https://doi.org/10.1016/j.neuron.2025.02.012

CellPress

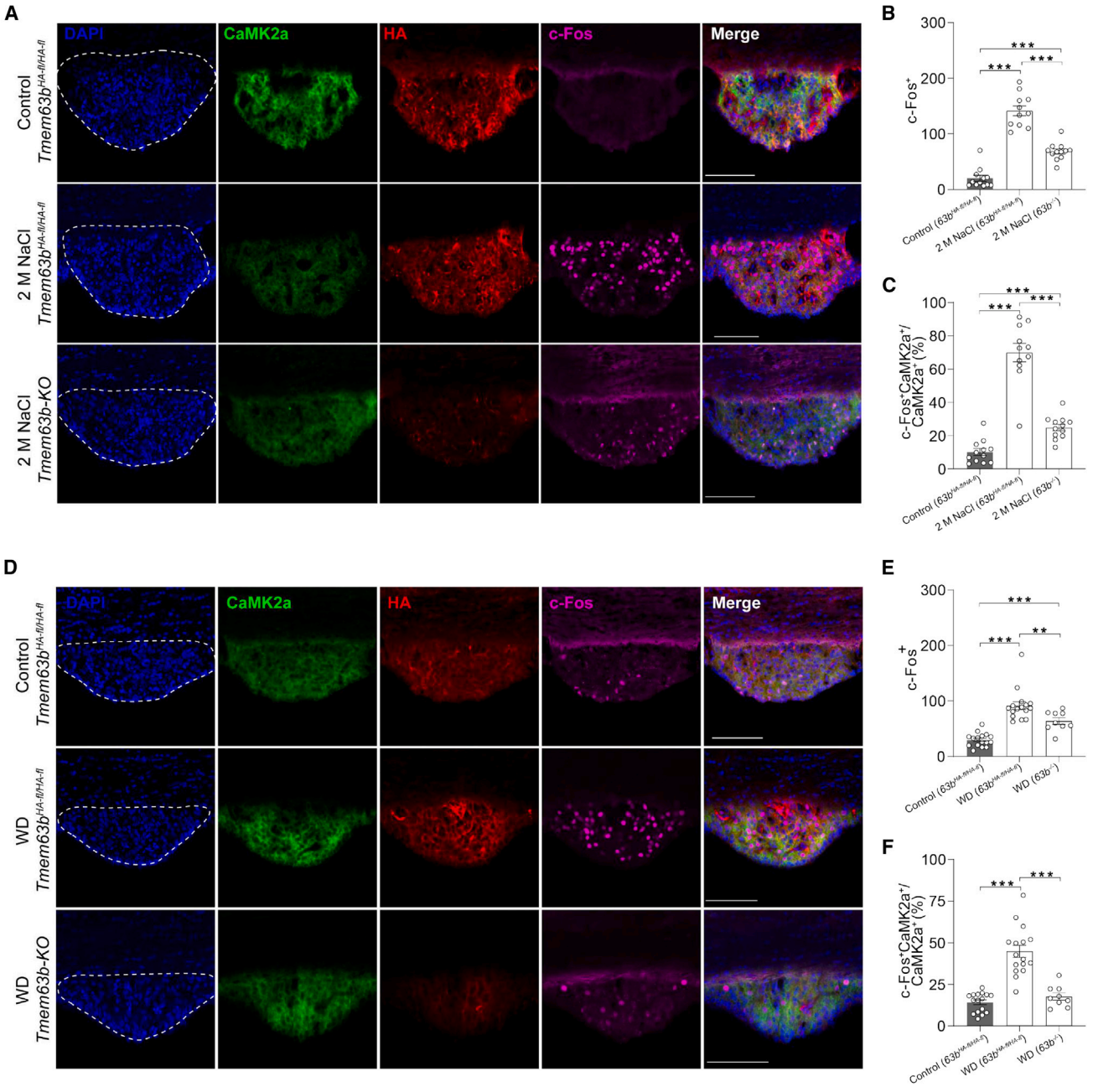

Figure 6. c-Fos immunostaining showed that TMEM63B is required for the activation of SFO excitatory neurons by osmotic or dehydration stress

(A and D) Representative images of the SFO region from *Tmem63b*$^{HA\text{-}fl/HA\text{-}fl}$ and *Tmem63b* knockout (KO) mice stained with antibodies against HA (red), CaMK2α (green), and c-Fos (purple) under osmotic (A) and dehydrated thirst (D) conditions. WD, water deprivation. Scale bar, 100 μm.

(B and E) Quantification of c-Fos-positive SFO neurons under both osmotic thirst (B) and dehydrated thirst (E) conditions. The number of c-Fos-positive cells increased under osmotic or dehydrated thirst conditions in *Tmem63b*$^{HA\text{-}fl/HA\text{-}fl}$ mice, and these increases were greatly reduced in *Tmem63b* KO mice.

(C and F) The co-labeling of c-Fos and CaMK2α in c-Fos-positive excitatory neurons. The percentage of c-Fos-positive excitatory neurons increased dramatically under osmotic (C) or dehydrated thirst (F) conditions in *Tmem63b*$^{HA\text{-}fl/HA\text{-}fl}$ mice, and these increases were greatly reduced in *Tmem63b* KO mice. For (A)–(F), control (*63b*$^{HA\text{-}fl/HA\text{-}fl}$) represents the untreated *Tmem63b*$^{HA\text{-}fl/HA\text{-}fl}$ mice. 2 M NaCl (*63b* $^{HA\text{-}fl/HA\text{-}fl}$) or WD (*63b* $^{HA\text{-}fl/HA\text{-}fl}$) denotes the *Tmem63b*$^{HA\text{-}fl/HA\text{-}fl}$ mice under osmotic or dehydrated thirst conditions. 2 M NaCl (*63b*$^{-/-}$) or WD (*63b*$^{-/-}$) indicates *Tmem63b*$^{-/-}$ mice under osmotic or dehydrated thirst conditions.

All error bars denote the mean ± SEM, $^{**}p < 0.01$, $^{***}p < 0.001$, Student's unpaired t test for (B) and (E), Mann-Whitney test for (C) and (F), $n = 9$–16, n represents the number of mice for (B) and (C) and (E) and (F).

Please cite this article in press as: Zou et al., TMEM63B functions as a mammalian hyperosmolar sensor for thirst, Neuron (2025), https://doi.org/10.1016/j.neuron.2025.02.012

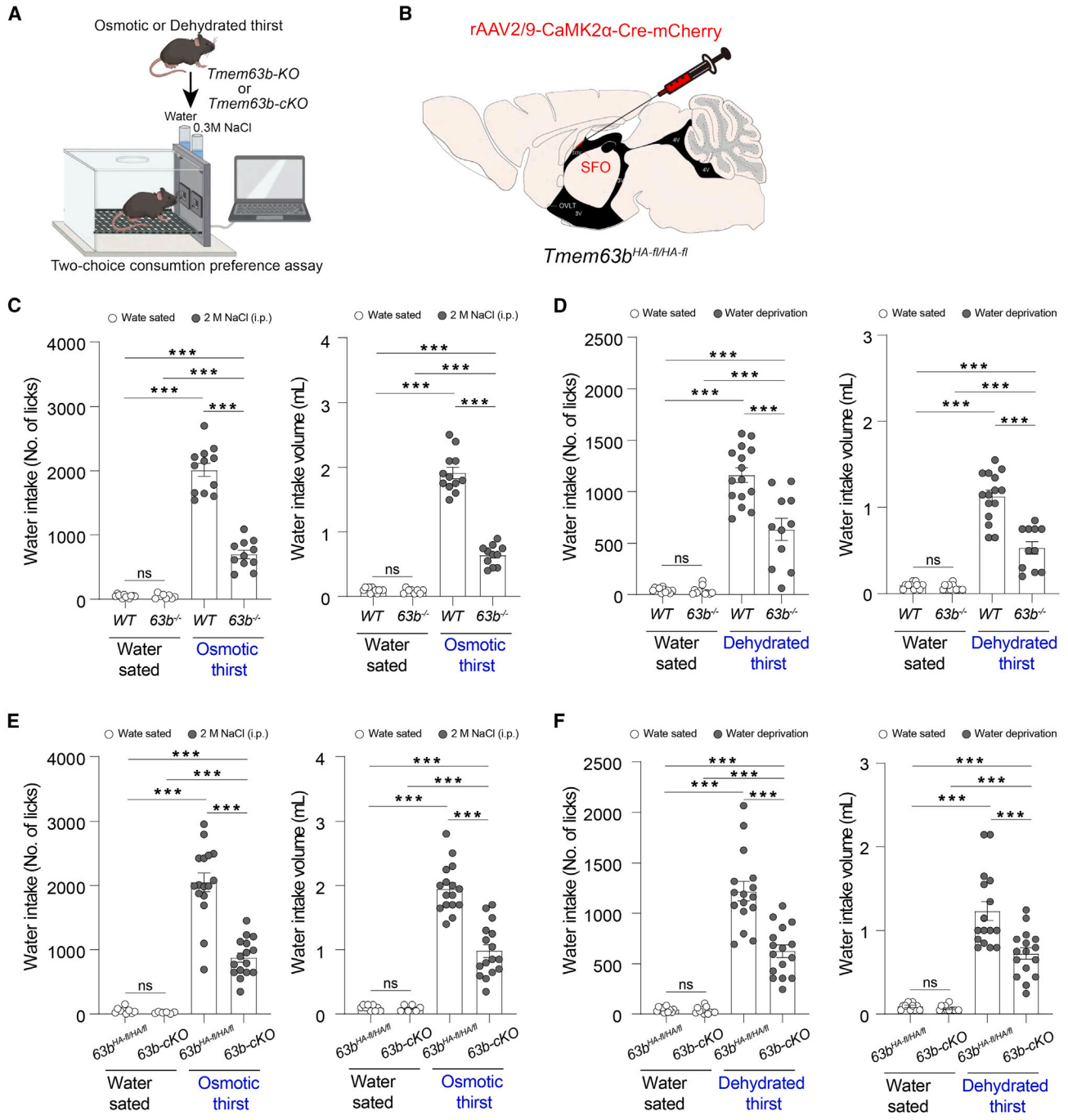

Figure 7. Conditional deletion of TMEM63B in SFO excitatory neurons profoundly impairs thirst behavior in mice

(A) Schematic diagram and experimental procedures of a two-choice consumption preference assay of osmotic or dehydrated thirst model mice.

(B) Schematic diagram of conditionally knocking out *Tmem63b* in SFO excitatory neurons by injecting AAV-CaMK2α-Cre-mCherry in the *Tmem63b*$^{HA\text{-}fl/HA\text{-}fl}$ SFO to generate *Tmem63b* cKO mice.

(C) Water intake of WT or *Tmem63b* KO (*Tmem63b*$^{-/-}$) mice during a 1-h session under a water-sated state or osmotic thirst conditions.

(D) The water intake of WT or *Tmem63b*$^{-/-}$ mice during a 1-h session under a water-sated state or dehydration.

(E) The water intake of *Tmem63b*$^{HA\text{-}fl/HA\text{-}fl}$ or *Tmem63b* cKO mice during a 1-h session under a water-sated state or osmotic thirst.

(F) The water intake of *Tmem63b*$^{HA\text{-}fl/HA\text{-}fl}$ or *Tmem63b* cKO mice during a 1-h session under a water-sated state or dehydration.

The number of licks and intake volume of water in *Tmem63b* KO or *Tmem63b* cKO mice were significantly reduced in both thirst models, whereas *Tmem63b* KO or *Tmem63b* cKO did not impair the basal water intake under the water-sated state. All error bars denote the mean ± SEM, $^{**}p < 0.01$, $^{***}p < 0.001$, Student's unpaired t test, n = 6–16, n represents the number of mice for (C)–(F).

deficits, and shortened lifespan.[63] Additionally, TMEM63B in the lamellar body, a lysosome-related organelle, is involved in storing pulmonary surfactant in alveolar epithelial (AT2) cells, a vital physiological function in preparing the lungs for maintaining respiration throughout life.[72] These findings provide a crucial molecular basis for exploring mechanosensitive processes in lysosomes.[63–65,72] Heterologously expressed TMEM63B in N2A and CHO cells was well localized in the plasma membrane (Figures S16A and A16B), as revealed by other studies,[72,74,83,84] and is partially co-localized with the lysosome marker lysosomal-associated membrane protein 1 (LAMP1) in N2A cells (Figure S16D), consistent with the previous study,[63,65] while this co-localization is relatively small in CHO cells (Figure S16E). Endogenous TMEM63B was predominantly expressed in the plasma membrane of SFO excitatory neurons (Figure S16C), and its co-localization with LAMP1 was barely detected (Figure S16F).

Thirst, the motivation driving animals to seek and consume fluid to restore water homeostasis, likely involves multiple pathways and signaling mechanisms. Conditional KO of *Tmem63b* in SFO excitatory neurons leads to a large impairment in thirst behavior (Figure 7), while the incomplete prevention of dehydration- or hyperosmolar-induced thirst in *Tmem63b* KO and cKO mice suggests alternative pathways and functional redundancy in hyperosmolar sensing for thirst. In the case of incomplete prevention of dehydration-induced thirst, the remaining thirst-driven behavior in *Tmem63b* KO mice could be caused by the angiotensin II receptor type 1a (AngII-Agtr1a) system, which is known to be involved in hypovolemic thirst[11,14,23] and can be activated by dehydration. Our further experiment showed that AngII can similarly lead to a calcium response in the SFO excitatory neurons of both control and *Tmem63b* cKO mice (Figures S7C–S7F), indicating that the two pathways operate in parallel. In the case of incomplete prevention of hyperosmolar-induced thirst, the thirst that remains in *Tmem63b* KO mice is induced by an unidentified mechanism independent of TMEM63B. One possibility may be related to the osmosensitive neurons in OVLT, as this brain region is another nucleus lying outside the blood-brain barrier besides SFO and is able to directly detect osmolarity changes in plasma, in which intrinsically osmosensitive neurons have been found.[32] TMEM63B is barely detected in OVLT (Figure S5C), suggesting that another molecular osmosensor may be responsible for this osmolarity-activated response in OVLT neurons and lead to thirst behavior. Further investigation is needed to elucidate the full spectrum of mechanisms governing thirst.

RESOURCE AVAILABILITY

Lead contact

Further information and requests for resources and reagents should be directed to and will be fulfilled by the lead contact, Zhiqiang Yan (zqyan@cimrbj.ac.cn).

Materials availability

All plasmids and genetically modified mice are available upon request.

Data and code availability

- The raw data presented in the study are available at Mendeley Data (https://www.doi.org/10.17632/c7k4xbs8zv.1).
- This paper does not report original code.
- Any additional information required to reanalyze the data reported in this paper is available from the lead contact upon request.

ACKNOWLEDGMENTS

We thank Yun Stone Shi at Guangdong Institute of Intelligence Science and Technology for the Tmem63bHA-fl/HA-fl mice. We thank Yulong Li at Peking University, Boxun Lu at Fudan University, Zhou-Feng Chen in Shenzhen Bay Laboratory, and Yi Lu and Cheng Zhong in Shenzhen Institute of Advanced Technology for comments. We thank the Bio-imaging Core of Shenzhen Bay Laboratory for providing imaging support. We also thank the Laboratory Animal Core of Shenzhen Bay Laboratory for providing mouse breeding and maintenance support. This work was supported by funds from the STI2030-Major Projects (2021ZD0203304), the Shenzhen Science and Technology Program (RCJC20210609104631084), the National Key R&D Program of China Project (2021YFA1101302), the National Natural Science Foundation of China (31970931), the Shenzhen Medical Research Funding (B2302032), and the National Natural Science Foundation of China (U23A20399).

AUTHOR CONTRIBUTIONS

W. Zou performed patch-clamp recording in cultured cells and brain slices as well as behavior tests and calcium imaging. S.D. performed patch-clamp recording experiments in cultured cells. X.C. mainly performed immunofluorescence staining, behavior tests, and calcium imaging. J.R. purified MmTMEM63B and conducted patch-clamp recording in recombinant proteoliposomes. H.W. performed calcium imaging. W. Zhan purified MmTMEM63B. J.W. and Z.L. performed single-cell RNA sequencing (RNA-seq) data analysis. Z.Y. initiated and supervised the study. Z.Y. and W. Zou designed the experiments. Z.Y., S.D., and W. Zou wrote the manuscript.

DECLARATION OF INTERESTS

We confirm that we have read the Journal's position on issues involved in ethical publication and affirm that this report is consistent with those guidelines.

STAR★METHODS

Detailed methods are provided in the online version of this paper and include the following:

- KEY RESOURCES TABLE
- EXPERIMENTAL MODEL AND STUDY PARTICIPANT DETAILS
  - Animals
  - Cell lines
- METHOD DETAILS
  - Induction of physiological states and behavioral assays
  - Ca^{2+} imaging
  - Immunohistochemistry
  - TMEM63B-eGFP expression and purification
  - Reconstitution of MmTMEM63B-eGFP in liposomes
  - Isolation and primary culture of SFO neurons
  - Patch-clamp recording
- QUANTIFICATION AND STATISTICAL ANALYSIS

SUPPLEMENTAL INFORMATION

Supplemental information can be found online at https://doi.org/10.1016/j.neuron.2025.02.012.

Received: October 9, 2024
Revised: January 28, 2025
Accepted: February 12, 2025
Published: March 18, 2025

REFERENCES

1. Noda, M., and Sakuta, H. (2013). Central regulation of body-fluid homeostasis. Trends Neurosci. *36*, 661–673. https://doi.org/10.1016/j.tins.2013.08.004.
2. Danziger, J., and Zeidel, M.L. (2015). Osmotic homeostasis. Clin. J. Am. Soc. Nephrol. *10*, 852–862. https://doi.org/10.2215/CJN.10741013.
3. Gizowski, C., and Bourque, C.W. (2018). The neural basis of homeostatic and anticipatory thirst. Nat. Rev. Nephrol. *14*, 11–25. https://doi.org/10.1038/nrneph.2017.149.
4. Zimmerman, C.A., Leib, D.E., and Knight, Z.A. (2017). Neural circuits underlying thirst and fluid homeostasis. Nat. Rev. Neurosci. *18*, 459–469. https://doi.org/10.1038/nrn.2017.71.
5. Augustine, V., Lee, S., and Oka, Y. (2020). Neural control and modulation of thirst, sodium appetite, and hunger. Cell *180*, 25–32. https://doi.org/10.1016/j.cell.2019.11.040.
6. Wolf, A.V. (1950). Osmometric analysis of thirst in man and dog. Am. J. Physiol. *161*, 75–86. https://doi.org/10.1152/ajplegacy.1950.161.1.75.
7. Fitzsimons, J.T. (1961). Drinking by rats depleted of body fluid without increase in osmotic pressure. J. Physiol. *159*, 297–309. https://doi.org/10.1113/jphysiol.1961.sp006809.
8. Fitzsimons, J.T. (1963). The effects of slow infusions of hypertonic solutions on drinking and drinking thresholds in rats. J. Physiol. *167*, 344–354. https://doi.org/10.1113/jphysiol.1963.sp007154.
9. Stricker, E.M. (1966). Extracellular fluid volume and thirst. Am. J. Physiol. *211*, 232–238. https://doi.org/10.1152/ajplegacy.1966.211.1.232.
10. Lehr, D., Mallow, J., and Krukowski, M. (1967). Copious drinking and simultaneous inhibition of urine flow elicited by beta-adrenergic stimulation and contrary effect of alpha-adrenergic stimulation. J. Pharmacol. Exp. Ther. *158*, 150–163.
11. Matsuda, T., Hiyama, T.Y., Niimura, F., Matsusaka, T., Fukamizu, A., Kobayashi, K., Kobayashi, K., and Noda, M. (2017). Distinct neural mechanisms for the control of thirst and salt appetite in the subfornical organ. Nat. Neurosci. *20*, 230–241. https://doi.org/10.1038/nn.4463.
12. Abbott, S.B.G., Machado, N.L.S., Geerling, J.C., and Saper, C.B. (2016). Reciprocal control of drinking behavior by median preoptic neurons in mice. J. Neurosci. *36*, 8228–8237. https://doi.org/10.1523/JNEUROSCI.1244-16.2016.
13. Oka, Y., Ye, M., and Zuker, C.S. (2015). Thirst driving and suppressing signals encoded by distinct neural populations in the brain. Nature *520*, 349–352. https://doi.org/10.1038/nature14108.
14. Zimmerman, C.A., Lin, Y.C., Leib, D.E., Guo, L., Huey, E.L., Daly, G.E., Chen, Y., and Knight, Z.A. (2016). Thirst neurons anticipate the homeostatic consequences of eating and drinking. Nature *537*, 680–684. https://doi.org/10.1038/nature18950.
15. Allen, W.E., DeNardo, L.A., Chen, M.Z., Liu, C.D., Loh, K.M., Fenno, L.E., Ramakrishnan, C., Deisseroth, K., and Luo, L. (2017). Thirst-associated preoptic neurons encode an aversive motivational drive. Science *357*, 1149–1155. https://doi.org/10.1126/science.aan6747.
16. Augustine, V., Gokce, S.K., Lee, S., Wang, B., Davidson, T.J., Reimann, F., Gribble, F., Deisseroth, K., Lois, C., and Oka, Y. (2018). Hierarchical neural architecture underlying thirst regulation. Nature *555*, 204–209. https://doi.org/10.1038/nature25488.
17. Pool, A.H., Wang, T., Stafford, D.A., Chance, R.K., Lee, S., Ngai, J., and Oka, Y. (2020). The cellular basis of distinct thirst modalities. Nature *588*, 112–117. https://doi.org/10.1038/s41586-020-2821-8.
18. Leib, D.E., Zimmerman, C.A., Poormoghaddam, A., Huey, E.L., Ahn, J.S., Lin, Y.C., Tan, C.L., Chen, Y., and Knight, Z.A. (2017). The forebrain thirst circuit drives drinking through negative reinforcement. Neuron *96*, 1272–1281.e4. https://doi.org/10.1016/j.neuron.2017.11.041.
19. Allen, W.E., Chen, M.Z., Pichamoorthy, N., Tien, R.H., Pachitariu, M., Luo, L., and Deisseroth, K. (2019). Thirst regulates motivated behavior through modulation of brainwide neural population dynamics. Science *364*, 253. https://doi.org/10.1126/science.aav3932.
20. Zhang, F., Mak, S.O.K., Liu, Y., Ke, Y., Rao, F., Yung, W.H., Zhang, L., and Chow, B.K.C. (2022). Secretin receptor deletion in the subfornical organ attenuates the activation of excitatory neurons under dehydration. Curr. Biol. *32*, 4832–4841.e5. https://doi.org/10.1016/j.cub.2022.09.037.
21. Liu, Y., Wei, J.A., Luo, Z., Cui, J., Luo, Y., Mak, S.O.K., Wang, S., Zhang, F., Yang, Y., So, K.F., et al. (2023). A gut-brain axis mediates sodium appetite via gastrointestinal peptide regulation on a medulla-hypothalamic circuit. Sci. Adv. *9*, eadd5330. https://doi.org/10.1126/sciadv.add5330.
22. Andersson, B., and McCann, S.M. (1956). The effect of hypothalamic lesions on the water intake of the dog. Acta Physiol. Scand. *35*, 312–320. https://doi.org/10.1111/j.1748-1716.1955.tb01288.x.
23. Simpson, J.B., and Routtenberg, A. (1973). Subfornical organ: site of drinking elicitation by angiotensin II. Science *181*, 1172–1175. https://doi.org/10.1126/science.181.4105.1172.
24. Andersson, B., Leksell, L.G., and Lishajko, F. (1975). Perturbations in fluid balance induced by medially placed forebrain lesions. Brain Res. *99*, 261–275. https://doi.org/10.1016/0006-8993(75)90028-1.
25. Buggy, J., and Jonhson, A.K. (1977). Preoptic-hypothalamic periventricular lesions: thirst deficits and hypernatremia. Am. J. Physiol. *233*, R44–R52. https://doi.org/10.1152/ajpregu.1977.233.1.R44.
26. McKinley, M.J., Denton, D.A., and Weisinger, R.S. (1978). Sensors for antidiuresis and thirst–osmoreceptors or CSF sodium detectors? Brain Res. *141*, 89–103. https://doi.org/10.1016/0006-8993(78)90619-4.
27. McKinley, M.J., Denton, D.A., Leksell, L.G., Mouw, D.R., Scoggins, B.A., Smith, M.H., Weisinger, R.S., and Wright, R.D. (1982). Osmoregulatory thirst in sheep is disrupted by ablation of the anterior wall of the optic recess. Brain Res. *236*, 210–215. https://doi.org/10.1016/0006-8993(82)90048-8.
28. Thrasher, T.N., Keil, L.C., and Ramsay, D.J. (1982). Lesions of the organum vasculosum of the lamina terminalis (OVLT) attenuate osmotically-induced drinking and vasopressin secretion in the dog. Endocrinology *110*, 1837–1839. https://doi.org/10.1210/endo-110-5-1837.
29. McKinley, M.J., McAllen, R.M., Davern, P., Giles, M.E., Penschow, J., Sunn, N., Uschakov, A., and Oldfield, B.J. (2003). The sensory circumventricular organs of the mammalian brain. Adv. Anat. Embryol. Cell Biol. *172*. III–XII. https://doi.org/10.1007/978-3-642-55532-9.
30. Sayer, R.J., Hubbard, J.I., and Sirett, N.E. (1984). Rat organum vasculosum laminae terminalis in vitro: responses to transmitters. Am. J. Physiol. *247*, R374–R379. https://doi.org/10.1152/ajpregu.1984.247.2.R374.
31. Sibbald, J.R., Hubbard, J.I., and Sirett, N.E. (1988). Responses from osmosensitive neurons of the rat subfornical organ in vitro. Brain Res. *461*, 205–214. https://doi.org/10.1016/0006-8993(88)90251-x.
32. Vivas, L., Chiaraviglio, E., and Carrer, H.F. (1990). Rat organum vasculosum laminae terminalis in vitro: responses to changes in sodium concentration. Brain Res. *519*, 294–300. https://doi.org/10.1016/0006-8993(90)90091-o.
33. Anderson, J.W., Washburn, D.L., and Ferguson, A.V. (2000). Intrinsic osmosensitivity of subfornical organ neurons. Neuroscience *100*, 539–547. https://doi.org/10.1016/s0306-4522(00)00313-4.
34. Faraco, G., Wijasa, T.S., Park, L., Moore, J., Anrather, J., and Iadecola, C. (2014). Water deprivation induces neurovascular and cognitive dysfunction through vasopressin-induced oxidative stress. J. Cereb. Blood Flow Metab. *34*, 852–860. https://doi.org/10.1038/jcbfm.2014.24.
35. Li, X.C., Shao, Y., and Zhuo, J.L. (2012). AT1a receptor signaling is required for basal and water deprivation-induced urine concentration in AT1a receptor-deficient mice. Am. J. Physiol. Ren. Physiol. *303*, F746–F756. https://doi.org/10.1152/ajprenal.00644.2011.
36. Coste, B., Mathur, J., Schmidt, M., Earley, T.J., Ranade, S., Petrus, M.J., Dubin, A.E., and Patapoutian, A. (2010). Piezo1 and Piezo2 are essential

components of distinct mechanically activated cation channels. Science *330*, 55–60. https://doi.org/10.1126/science.1193270.

37. Coste, B., Xiao, B., Santos, J.S., Syeda, R., Grandl, J., Spencer, K.S., Kim, S.E., Schmidt, M., Mathur, J., Dubin, A.E., et al. (2012). Piezo proteins are pore-forming subunits of mechanically activated channels. Nature *483*, 176–181. https://doi.org/10.1038/nature10812.

38. Syeda, R., Florendo, M.N., Cox, C.D., Kefauver, J.M., Santos, J.S., Martinac, B., and Patapoutian, A. (2016). Piezo1 channels are inherently mechanosensitive. Cell Rep. *17*, 1739–1746. https://doi.org/10.1016/j.celrep.2016.10.033.

39. Murthy, S.E., Dubin, A.E., Whitwam, T., Jojoa-Cruz, S., Cahalan, S.M., Mousavi, S.A.R., Ward, A.B., and Patapoutian, A. (2018). OSCA/TMEM63 are an evolutionarily conserved family of mechanically activated ion channels. eLife *7*, e41844. https://doi.org/10.7554/eLife.41844.

40. Jojoa-Cruz, S., Saotome, K., Murthy, S.E., Tsui, C.C.A., Sansom, M.S., Patapoutian, A., and Ward, A.B. (2018). Cryo-EM structure of the mechanically activated ion channel OSCA1.2. eLife *7*, e41845. https://doi.org/10.7554/eLife.41845.

41. Douguet, D., and Honoré, E. (2019). Mammalian mechanoelectrical transduction: structure and function of force-gated ion channels. Cell *179*, 340–354. https://doi.org/10.1016/j.cell.2019.08.049.

42. Du, H., Ye, C., Wu, D., Zang, Y.Y., Zhang, L., Chen, C., He, X.Y., Yang, J.J., Hu, P., Xu, Z., et al. (2020). The cation channel TMEM63B is an osmosensor required for hearing. Cell Rep. *31*, 107596. https://doi.org/10.1016/j.celrep.2020.107596.

43. Jia, Y., Zhao, Y., Kusakizako, T., Wang, Y., Pan, C., Zhang, Y., Nureki, O., Hattori, M., and Yan, Z. (2020). TMC1 and TMC2 proteins are pore-forming subunits of mechanosensitive ion channels. Neuron *105*, 310–321.e3. https://doi.org/10.1016/j.neuron.2019.10.017.

44. Kefauver, J.M., Ward, A.B., and Patapoutian, A. (2020). Discoveries in structure and physiology of mechanically activated ion channels. Nature *587*, 567–576. https://doi.org/10.1038/s41586-020-2933-1.

45. Jin, P., Jan, L.Y., and Jan, Y.N. (2020). Mechanosensitive ion channels: structural features relevant to mechanotransduction mechanisms. Annu. Rev. Neurosci. *43*, 207–229. https://doi.org/10.1146/annurev-neuro-070918-050509.

46. Xiao, B. (2020). Levering mechanically activated Piezo channels for potential pharmacological intervention. Annu. Rev. Pharmacol. Toxicol. *60*, 195–218. https://doi.org/10.1146/annurev-pharmtox-010919-023703.

47. Li, Q., and Montell, C. (2021). Mechanism for food texture preference based on grittiness. Curr. Biol. *31*, 1850–1861.e6. https://doi.org/10.1016/j.cub.2021.02.007.

48. Zheng, W., and Holt, J.R. (2021). The mechanosensory transduction machinery in inner ear hair cells. Annu. Rev. Biophys. *50*, 31–51. https://doi.org/10.1146/annurev-biophys-062420-081842.

49. Li, S., Li, B., Gao, L., Wang, J., and Yan, Z. (2022). Humidity response in Drosophila olfactory sensory neurons requires the mechanosensitive channel TMEM63. Nat. Commun. *13*, 3814. https://doi.org/10.1038/s41467-022-31253-z.

50. Jeong, H., Clark, S., Goehring, A., Dehghani-Ghahnaviyeh, S., Rasouli, A., Tajkhorshid, E., and Gouaux, E. (2022). Structures of the TMC-1 complex illuminate mechanosensory transduction. Nature *610*, 796–803. https://doi.org/10.1038/s41586-022-05314-8.

51. Poole, K. (2022). The diverse physiological functions of mechanically activated ion channels in mammals. Annu. Rev. Physiol. *84*, 307–329. https://doi.org/10.1146/annurev-physiol-060721-100935.

52. Zheng, W., Rawson, S., Shen, Z., Tamilselvan, E., Smith, H.E., Halford, J., Shen, C., Murthy, S.E., Ulbrich, M.H., Sotomayor, M., et al. (2023). TMEM63 proteins function as monomeric high-threshold mechanosensitive ion channels. Neuron *111*, 3195–3210.e7. https://doi.org/10.1016/j.neuron.2023.07.006.

53. Zhang, M., Shan, Y., Cox, C.D., and Pei, D. (2023). A mechanical-coupling mechanism in OSCA/TMEM63 channel mechanosensitivity. Nat. Commun. *14*, 3943. https://doi.org/10.1038/s41467-023-39688-8.

54. Hou, C., Tian, W., Kleist, T., He, K., Garcia, V., Bai, F., Hao, Y., Luan, S., and Li, L. (2014). DUF221 proteins are a family of osmosensitive calcium-permeable cation channels conserved across eukaryotes. Cell Res. *24*, 632–635. https://doi.org/10.1038/cr.2014.14.

55. Yuan, F., Yang, H., Xue, Y., Kong, D., Ye, R., Li, C., Zhang, J., Theprungsirikul, L., Shrift, T., Krichilsky, B., et al. (2014). OSCA1 mediates osmotic-stress-evoked Ca^{2+} increases vital for osmosensing in Arabidopsis. Nature *514*, 367–371. https://doi.org/10.1038/nature13593.

56. Zhang, M., Wang, D., Kang, Y., Wu, J.X., Yao, F., Pan, C., Yan, Z., Song, C., and Chen, L. (2018). Structure of the mechanosensitive OSCA channels. Nat. Struct. Mol. Biol. *25*, 850–858. https://doi.org/10.1038/s41594-018-0117-6.

57. Liu, X., Wang, J., and Sun, L. (2018). Structure of the hyperosmolality-gated calcium-permeable channel OSCA1.2. Nat. Commun. *9*, 5060. https://doi.org/10.1038/s41467-018-07564-5.

58. Maity, K., Heumann, J.M., McGrath, A.P., Kopcho, N.J., Hsu, P.K., Lee, C.W., Mapes, J.H., Garza, D., Krishnan, S., Morgan, G.P., et al. (2019). Cryo-EM structure of OSCA1.2 from Oryza sativa elucidates the mechanical basis of potential membrane hyperosmolality gating. Proc. Natl. Acad. Sci. USA *116*, 14309–14318. https://doi.org/10.1073/pnas.1900774116.

59. Han, Y., Wang, Y., Zhai, Y., Wen, Z., Liu, J., Xi, C., Zhao, H., Wang, Y., and Han, S. (2022). OsOSCA1.1 mediates hyperosmolality and salt stress sensing in Oryza sativa. Biology *11*, 678. https://doi.org/10.3390/biology11050678.

60. Han, Y., Zhou, Z., Jin, R., Dai, F., Ge, Y., Ju, X., Ma, X., He, S., Yuan, L., Wang, Y., et al. (2024). Mechanical activation opens a lipid-lined pore in OSCA ion channels. Nature *628*, 910–918. https://doi.org/10.1038/s41586-024-07256-9.

61. Shan, Y., Zhang, M., Chen, M., Guo, X., Li, Y., Zhang, M., and Pei, D. (2024). Activation mechanisms of dimeric mechanosensitive OSCA/TMEM63 channels. Nat. Commun. *15*, 7504. https://doi.org/10.1038/s41467-024-51800-0.

62. Pei, S., Tao, Q., Li, W., Qi, G., Wang, B., Wang, Y., Dai, S., Shen, Q., Wang, X., Wu, X., et al. (2024). Osmosensor-mediated control of $Ca^{(2+)}$ spiking in pollen germination. Nature *629*, 1118–1125. https://doi.org/10.1038/s41586-024-07445-6.

63. Li, K., Guo, Y., Wang, Y., Zhu, R., Chen, W., Cheng, T., Zhang, X., Jia, Y., Liu, T., Zhang, W., et al. (2024). Drosophila TMEM63 and mouse TMEM63A are lysosomal mechanosensory ion channels. Nat. Cell Biol. *26*, 393–403. https://doi.org/10.1038/s41556-024-01353-7.

64. Jan, L.Y., and Jan, Y.N. (2025). Wide-ranging cellular functions of ion channels and lipid scramblases in the structurally related TMC, TMEM16 and TMEM63 families. Nat. Struct. Mol. Biol. *32*, 222–236. https://doi.org/10.1038/s41594-024-01444-x.

65. Li, K., and Jan, Y.N. (2025). Experimental tools and emerging principles of organellar mechanotransduction. Trends Cell Biol. S0962-8924(24)00279-4. https://doi.org/10.1016/j.tcb.2024.12.011.

66. Yan, H., Helman, G., Murthy, S.E., Ji, H., Crawford, J., Kubisiak, T., Bent, S.J., Xiao, J., Taft, R.J., Coombs, A., et al. (2019). Heterozygous variants in the mechanosensitive ion channel TMEM63A result in transient hypomyelination during infancy. Am. J. Hum. Genet. *105*, 996–1004. https://doi.org/10.1016/j.ajhg.2019.09.011.

67. Wu, D., Zang, Y.Y., Shi, Y.Y., Ye, C., Cai, W.M., Tang, X.H., Zhao, L., Liu, Y., Gan, Z., Chen, G.Q., et al. (2020). Distant coupling between RNA editing and alternative splicing of the osmosensitive cation channel Tmem63b. J. Biol. Chem. *295*, 18199–18212. https://doi.org/10.1074/jbc.RA120.016049.

68. Fukumura, S., Hiraide, T., Yamamoto, A., Tsuchida, K., Aoto, K., Nakashima, M., and Saitsu, H. (2022). A novel de novo TMEM63A variant

in a patient with severe hypomyelination and global developmental delay. Brain Dev. *44*, 178–183. https://doi.org/10.1016/j.braindev.2021.09.006.

69. Tábara, L.C., Al-Salmi, F., Maroofian, R., Al-Futaisi, A.M., Al-Murshedi, F., Kennedy, J., Day, J.O., Courtin, T., Al-Khayat, A., Galedari, H., et al. (2022). TMEM63C mutations cause mitochondrial morphology defects and underlie hereditary spastic paraplegia. Brain *145*, 3095–3107. https://doi.org/10.1093/brain/awac123.
70. Qin, Y., Yu, D., Wu, D., Dong, J., Li, W.T., Ye, C., Cheung, K.C., Zhang, Y., Xu, Y., Wang, Y., et al. (2023). Cryo-EM structure of TMEM63C suggests it functions as a monomer. Nat. Commun. *14*, 7265. https://doi.org/10.1038/s41467-023-42956-2.
71. Vetro, A., Pelorosso, C., Balestrini, S., Masi, A., Hambleton, S., Argilli, E., Conti, V., Giubbolini, S., Barrick, R., Bergant, G., et al. (2023). Stretch-activated ion channel TMEM63B associates with developmental and epileptic encephalopathies and progressive neurodegeneration. Am. J. Hum. Genet. *110*, 1356–1376. https://doi.org/10.1016/j.ajhg.2023.06.008.
72. Chen, G.L., Li, J.Y., Chen, X., Liu, J.W., Zhang, Q., Liu, J.Y., Wen, J., Wang, N., Lei, M., Wei, J.P., et al. (2024). Mechanosensitive channels TMEM63A and TMEM63B mediate lung inflation-induced surfactant secretion. J. Clin. Invest. *134*, e174508. https://doi.org/10.1172/JCI174508.
73. Yang, G., Jia, M., Li, G., Zang, Y.Y., Chen, Y.Y., Wang, Y.Y., Zhan, S.Y., Peng, S.X., Wan, G., Li, W., et al. (2024). TMEM63B channel is the osmosensor required for thirst drive of interoceptive neurons. Cell Discov. *10*, 1. https://doi.org/10.1038/s41421-023-00628-x.
74. Wu, D., Xu, L., Cai, W.M., Zhan, S.Y., Wan, G., Xu, Y., and Shi, Y.S. (2023). A splicing-dependent ER retention signal regulates surface expression of the mechanosensitive TMEM63B cation channel. J. Biol. Chem. *299*, 102781. https://doi.org/10.1016/j.jbc.2022.102781.
75. Bourque, C.W. (2008). Central mechanisms of osmosensation and systemic osmoregulation. Nat. Rev. Neurosci. *9*, 519–531. https://doi.org/10.1038/nrn2400.
76. Zimmerman, C.A., Huey, E.L., Ahn, J.S., Beutler, L.R., Tan, C.L., Kosar, S., Bai, L., Chen, Y., Corpuz, T.V., Madisen, L., et al. (2019). A gut-to-brain signal of fluid osmolarity controls thirst satiation. Nature *568*, 98–102. https://doi.org/10.1038/s41586-019-1066-x.
77. Ichiki, T., Wang, T., Kennedy, A., Pool, A.H., Ebisu, H., Anderson, D.J., and Oka, Y. (2022). Sensory representation and detection mechanisms of gut osmolality change. Nature *602*, 468–474. https://doi.org/10.1038/s41586-021-04359-5.
78. Grove, J.C.R., Gray, L.A., La Santa Medina, N., Sivakumar, N., Ahn, J.S., Corpuz, T.V., Berke, J.D., Kreitzer, A.C., and Knight, Z.A. (2022). Dopamine subsystems that track internal states. Nature *608*, 374–380. https://doi.org/10.1038/s41586-022-04954-0.
79. Matsuda, T., Hiyama, T.Y., Kobayashi, K., Kobayashi, K., and Noda, M. (2020). Distinct CCK-positive SFO neurons are involved in persistent or transient suppression of water intake. Nat. Commun. *11*, 5692. https://doi.org/10.1038/s41467-020-19191-0.
80. Arnadóttir, J., and Chalfie, M. (2010). Eukaryotic mechanosensitive channels. Annu. Rev. Biophys. *39*, 111–137. https://doi.org/10.1146/annurev.biophys.37.032807.125836.
81. Fukasaku, M., Kimura, J., and Yamaguchi, O. (2016). Swelling-activated and arachidonic acid-induced currents are TREK-1 in rat bladder smooth muscle cells. Fukushima J. Med. Sci. *62*, 18–26. https://doi.org/10.5387/fms.2015-20.
82. Liu, X., Huang, H., Wang, W., Wang, J., Sachs, F., and Niu, W. (2008). Stretch-activated potassium channels in hypotonically induced blebs of atrial myocytes. J. Membr. Biol. *226*, 17–25. https://doi.org/10.1007/s00232-008-9135-3.
83. Marques, M.C., Albuquerque, I.S., Vaz, S.H., and Bernardes, G.J.L. (2019). Overexpression of osmosensitive $Ca^{(2+)}$-permeable channel TMEM63B promotes migration in HEK293T cells. Biochemistry *58*, 2861–2866. https://doi.org/10.1021/acs.biochem.9b00224.
84. Miyata, Y., Takahashi, K., Lee, Y., Sultan, C.S., Kuribayashi, R., Takahashi, M., Hata, K., Bamba, T., Izumi, Y., Liu, K., et al. (2025). Membrane structure-responsive lipid scrambling by TMEM63B to control plasma membrane lipid distribution. Nat. Struct. Mol. Biol. *32*, 185–198. https://doi.org/10.1038/s41594-024-01411-6.
85. Battle, A.R., Petrov, E., Pal, P., and Martinac, B. (2009). Rapid and improved reconstitution of bacterial mechanosensitive ion channel proteins MscS and MscL into liposomes using a modified sucrose method. FEBS Lett. *583*, 407–412. https://doi.org/10.1016/j.febslet.2008.12.033.

Please cite this article in press as: Zou et al., TMEM63B functions as a mammalian hyperosmolar sensor for thirst, Neuron (2025), https://doi.org/10.1016/j.neuron.2025.02.012

STAR★METHODS

KEY RESOURCES TABLE

REAGENT or RESOURCE	SOURCE	IDENTIFIER
Antibodies		
HA-Tag (Rabbit mAb)	Cell Signaling Technology	Cat# 3724S; RRID: AB_1546585
HA-Tag (Mouse IgG1)	Sigma-Aldrich	Cat# H3663; RRID: AB_262051
CaMK2α (Rabbit IgG)	Abcam	Cat# ab92332; RRID: AB_2049246
c-Fos (Rat IgG2a)	Synaptic Systems	Cat# 226017; RRID: AB_2864765
Rabbit anti-FLAG	Cell Signaling Technology	Cat# 2368T; RRID: AB_2217020
Rat anti-LAMP1	Santa Cruz	Cat# sc-19992; RRID: AB_2134495
Bacterial and virus strains		
rAAV2/9-CaMK2α-mCherry	BrainVTA	N/A
rAAV2/9-CaMK2α-Cre-mCherry	BrainVTA	N/A
rAAV2/9-CaMK2α-GCaMP6f-P2A-Cre	BrainVTA	N/A
rAAV2/9-CaMK2α-GCaMP6f	BrainVTA	N/A
rAAV2/9-CaMK2α-TMEM63B-P2A-eGFP	This study	N/A
Chemicals, peptides, and recombinant proteins		
Phenylmethylsulfonyl	Beyotime	Cat# ST507
Dithiothreitol	Sigma-Aldrich	Cat# D0632
Anti-DYKDDDDK affinity beads	Smart-Life sciences	Cat# SA042025
Soy phospholipids	Sigma-Aldrich	Cat# 11145
DDM	Anatrace	Cat# 69227-93-6
CHS	Anatrace	Cat# CH210
Protease inhibitor cocktail	Sigma-Aldrich	Cat# S8830
Salts, acids, bases for recording and imaging solutions	Sigma-Aldrich	Stock
Deposited data		
Raw and analyzed data	This paper	Mendeley Data: https://www.doi.org/10.17632/c7k4xbs8zv.1
Experimental models: Cell lines		
Neuro-2a cell	American Type Culture Collection (ATCC)	ATCC CCL-131; RRID: CVCL_0470
CHO cell	American Type Culture Collection (ATCC)	ATCC CCL-61; RRID: CVCL_0214
HEK293T cell	American Type Culture Collection (ATCC)	ATCC CRL-1573; RRID: CVCL_0045
HEK293F cell	American Type Culture Collection (ATCC)	ATCC CRL-3537; RRID: CVCL_4V95
Experimental models: Organisms/strains		
Mouse: *Tmem63b*$^{-/-}$	This Paper	N/A
Mouse: *Tmem63b*$^{HA\text{-}fl/+}$	From Yun Stone Shi	N/A
Recombinant DNA		
HsTMEM63B	This Paper	GeneBank: NM_001318792.1
MmTmem63b	This Paper	GeneBank: NM_198167
MmTrek1	This Paper	GeneBank: NM_001159850.2
Software and algorithms		
PClamp 11 software suite	Molecular Devices	https://www.moleculardevices.com
Patchmaster	HEKA Electronic	http://www.heka.com/
GraphPad Prism 8.0.2	GraphPad Software	https://www.graphpad.com
Clustal Omega sequence	European Bioinformatics	https://www.ebi.ac.uk/Tools/msa/clust

(*Continued on next page*)

Please cite this article in press as: Zou et al., TMEM63B functions as a mammalian hyperosmolar sensor for thirst, Neuron (2025), https://doi.org/10.1016/j.neuron.2025.02.012

Continued

REAGENT or RESOURCE	SOURCE	IDENTIFIER
Imaris 9.9	Oxford Instruments	https://imaris.oxinst.cn
SPSS 22.0	IBM	https://www.ibm.com/uk-en/analytics/spss-statistics-software
Other		
Borosilicate glass pipettes	Sutter Instrument	Cat# BF150-86-10

EXPERIMENTAL MODEL AND STUDY PARTICIPANT DETAILS

Animals

Mice were bred and maintained in standard cages under a condition of 12-hours light-dark cycle in a specific-pathogen-free (SPF) animal facility accredited by the Association for Assessment and Accreditation of Laboratory Animal Care (AAALAC). All the animal experiments involving the operation on mice were rigidly conducted by the animal protocols, approved by the Institutional Animal Care and Use Committee of the animal facility of the Model Animal Research Center of Shenzhen Bay Laboratory, Shenzhen, China. Both male and female animals were unbiasedly used in all the animal experiments. Mice from 5 weeks old and 8-12 weeks old were used in this study. Detailed information is indicated in the figures and legends. *Tmem63b*$^{HA\text{-}fl/+}$ mice were given by Yun Stone Shi.[42] *Tmem63b* knockout (*Tmem63b*$^{-/-}$) mice were generated by mating *Tmem63b*$^{HA\text{-}fl/+}$ and CMV-Cre (Jackson NO. 006054) mice.

Cell lines

Neuro2a (N2a) and HEK293T cells were grown in Dulbecco's Modified Eagle Medium (DMEM) containing 4.5 mg/ml glucose, and 10% fetal bovine serum (GIBCO, USA). CHO cells were grown in DMEM/F12 containing 15 mM HEPES and 10% fetal bovine serum. HEK293F cells were grown in SMM 293-TII medium. All cell lines were cultured at 37°C.

METHOD DETAILS

Induction of physiological states and behavioral assays

For the osmotic thirst experiments, the mice were water deprivation for 24 hours to train in the Skinner box and were handled the next day. Then, the mice were injected with 2 M NaCl (5 μl/g body weight, i.p.) and subjected to 10 minutes of water and food deprivation before behavioral testing. In moderate osmotic thirst model, the mice were injected with 1M NaCl (5 μl/g body weight, i.p.) and subjected to 10 minutes of water and food deprivation before behavioral testing. For the c-Fos staining, mice were kept in the home cage without access to food or water for 1 h to allow for stimulus-induced expression of immediate early genes.

For the water deprivation experiments, the trained and handled mice were fed food and 1 ml of water daily for 48 hours. In moderate dehydrated thirst model, the trained and handled mice were fed food and 1 ml of water daily for 36 hours. After that, the mice were subjected to behavioral testing or euthanized for c-Fos staining.

For *Tmem63b* conditional knockout mice, rAAV2/9-CaMK2α-Cre-mCherry was injected to the SFO to selectively knockout TMEM63B in SFO excitatory neuron. For TMEM63B-overexpressed mice, rAAV2/9-CaMK2α-TMEM63B-P2A-eGFP was injected to the SFO to overexpress TMEM63B in SFO excitatory neuron. Mice were subjected to behavioral test three weeks after virus injection. All of the behavioral assays were performed in a custom Skinner box (Beijing Zhongshi Dichuang Technology Development Co., Ltd) with different paradigms unless otherwise noted. The mice were trained in the Skinner box under water deprivation for 24 hours before the behavioral assays to train. As previously described,[17] for the two-choice consumption preference assay, one bottle of water and one bottle of 0.3 M NaCl were presented in sequence during the same session. Mice in different groups were recorded for 1 hour, and the number of licks toward different solutions was measured.

Ca^{2+} imaging

For N2A cells, cytoplasmic calcium levels were monitored using GCaMP6f. To form a tandem expression system, GCaMP6f was added to the C-terminus of HsTMEM63B via a P2A linker (TMEM63B-P2A-GCaMP6f-IRES-mCherry). The pCMV6-TMEM63B-P2A-GCaMP6f-IRES-mCherry vector was transfected into Neuro-2a cells prepared on the cell slide, and the pCMV6-GCaMP6f-IRES-mCherry vector was used as a control. After a 48 h transfection, the cells were perfused with extracellular solutions of varying osmolarities at a constant exchange speed using a peristaltic pump. Calcium fluorescence images were obtained at 0.5 Hz for 10 min using a laser scanning confocal microscope (Nikon A1, Japan) with a 20X objective lens and an excitation wavelength of 488 nm and 561 nm at room temperature (24 ± 2 °C). Cells were recorded in the isotonic solution for 2 min, switched to hypertonic solution for 4 min, and then switched back to isotonic solution for another 4 min. The isotonic solution (300 mOsm/kg) contained (mM): 72 NaCl, 5 KCl, 1 $CaCl_2$, 1 $MgCl_2$, 10 HEPES, 130 mannitol, pH 7.4 adjusted with NaOH. Additional hypoosmotic and hyperosmotic solutions

Please cite this article in press as: Zou et al., TMEM63B functions as a mammalian hyperosmolar sensor for thirst, Neuron (2025), https://doi.org/10.1016/j.neuron.2025.02.012

were prepared by adjusting the solutions with mannitol without changing the ion concentrations. The osmolarity of the solutions was measured using a freezing point osmometer (Gonotec, 3000 Basci, Germany).

For calcium imaging in brain slices. Adult mice were injected with AAV-CaMK2a-GCaMP6f-mCherry and AAV-CaMK2a-GCaMP6f-Cre-mCherry virus into SFO. Three weeks after virus injection, calcium imaging of SFO slices was conducted at 1 Hz for 15 min using an Olympus FVMPE-RS microscope equipped with a Spectra-Physica InSight X3 dual-output laser. 1 μM AngII in ACSF was bath-applied using a slow perfusion system (2 ml min^{-1}) during imaging.

Time-lapse images were analyzed to acquire the fluorescence intensity in the region of interest (ROI) in each frame. The change in fluorescence intensity $\Delta F/F_0$ was calculated as $100\% * (F_t-F_0)/F_0$, where F_t was the fluorescence intensity at time t and F_0 was the average fluorescence intensity prior to the application of the osmolarity stimulus.

Immunohistochemistry

For immunostaining of brain slices, mice were deeply anesthetized with pentobarbital sodium (50 mg/kg) and perfused with PBS followed by 4% paraformaldehyde (PFA, pH 7.4). Mouse brains were extracted, then fixed overnight at 4℃ in 4% PFA and coronally sectioned at 35 μm intervals using a freezing microtome (CM3050S, Leica). Brain sections were permeabilized with a solution containing 5% bovine serum albumin and 1% Triton X-100 in PBS for 40 minutes at room temperature. For non-permeablized staining, the step of incubating the brain section in a 1% Triton X-100 solution was omitted. Then the sections were blocked with a solution of 5% bovine serum albumin in PBS for 2 hours at room temperature followed by overnight primary antibody (1% bovine serum albumin in PBS) at 4℃. The following primary antibodies were used: rabbit anti-HA-Tag (1:100, Cell Signaling Technology 3724S), mouse anti-HA-Tag (1:500, rabbit Sigma-Aldrich H3663), anti-FLAG (1:50, CST 2368T), rabbit anti-CaMK2α (1:1000, Abcam ab92332), rat anti-c-Fos (1:2500, Synaptic Systems 226017), and rabbit anti-TMEM63B (1:1000, custom-made affinity-purified polyclonal antibody with antigen sequence of TDADRLRRQERERVC). After washing three times with PBS, the brain sections were stained with secondary antibody for 2 hours at room temperature. The following secondary antibodies (1:1000, Thermo Fisher Scientific) were used: Alexa Fluor 488 Goat anti-Mouse (A11029), Alexa Fluor 488 Goat anti-Rabbit (A11008), Alexa Fluor 568 Goat anti-Mouse (A11031), Alexa Fluor 568 Goat anti-Rabbit (A11036), Alexa Fluor 647 Goat anti-Rat (A48265). DAPI (5 μg/ml) was then incubated for 5 min at room temperature. Following three additional washes with PBS, the brain sections were mounted on glass slides and imaged on a confocal microscope (Nikon A1). Cell counting was performed using Imaris (version 9.9).

For immunostaining in culture cells, CHO or N2A cells were transfected with plasmids on matrigel-coated coverslips for around 24 h. pCMV-HA-HsTMEM63B-ires-eGFP was used for non-permeabilized staining while pCMV-HA-HsTMEM63B-eGFP was used for permeabilized staining. Cells were treated with 4% paraformaldehyde (PFA) solution for 15 min at room temperature (25℃) and 1% Triton X-100 in PBS for 15 minutes at room temperature. For non-permeablized staining, the step of incubating cells in a 1% Triton X-100 solution was omitted. Then the cells were blocked with a solution of 5% bovine serum albumin in PBS for 2 hours at room temperature and incubated overnight in the primary antibody: anti-HA rabbit polyclonal antibody (1:1000, Cell Signaling Technology, 3724), anti-LAMP1 rat monoclonal antibody (1:500, Santa Cruz, sc-19992). After washing three times with PBS, the following secondary antibodies (1:1000, Thermo Fisher Scientific) were used: Alexa Fluor 568 Goat anti-Rabbit (A11036) and Fluor 647 Goat anti-Rat (A48265). Following three additional washes with PBS, the coverslips were mounted on glass slides and imaged on a confocal microscope (Nikon A1).

TMEM63B-eGFP expression and purification

The *MmTmem63b* (NM_198167) gene was synthesized by GenScript and subcloned and inserted into the vector pCDNA3.1-eGFP. A 3×FLAG tag (DYKDHDGDYKDHDI DYKDDDDK) was added to the C-terminus of the *MmTmem63b* gene with a GSAGS linker. The MmTMEM63B protein used for reconstitution was expressed in HEK293F cells. For protein expression and purification, HEK293F cells were grown in SMM 293-TII medium to a density of 1.8×10^6 cells/mL and transfected with 1 μg DNA and 3 μl 1 mg/mL PEI in 20 mL of Opti-MEM. HEK293F cells were cultured for 60 hours at 37°C and then harvested and pelleted. The pellets were washed with ice-cold PBS and stored at -80 °C for future use. The pellets were thawed on ice and sonicated in 50 mM Tris-HCl (pH 7.5), 150 mM NaCl with 1 mM phenylmethylsulfonyl fluoride, protease inhibitor cocktail (Sigma, S8830) and 1 mM dithiothreitol (DTT, Sigma D0632). Then, the cell lysate was incubated with SuperNuclease at 4 °C for 5 minutes, 2% DDM and 0.4% CHS were added, and the solutions were stirred for 2 hours. Insoluble material was removed by ultracentrifugation for 45 min at 40000 g (Beckman, JA-25.50 rotor), and the supernatant was loaded onto Anti-DYKDDDDK affinity beads (Smart-Life Sciences, SA042025). After the beads were washed with 50 mM Tris (pH 7.5), 150 mM NaCl, 0.05% DDM, 0.01% CHS, and 1 mM DTT, the protein was eluted with 50 mM Tris (pH 7.5), 150 mM NaCl, 0.05% DDM, 0.01% CHS, 200 μg/mL 3× FLAG peptide, and 1 mM DTT. The sample was concentrated using a 100 kDa MWCO Amicon Ultracentrifugal filter (Millipore, UFC910096) and then applied to a Superose™ 6 Increase 10/300 GL (Cytiva, 29091596) equilibrated with a buffer containing 50 mM Tris-HCl (pH 7.5), 150 mM NaCl, 0.05% DDM, 0.01% CHS, and 1 mM DTT. The peak fractions corresponding to MmTMEM63B-eGFP were concentrated at 1 mg/mL. The proteins were aliquoted and stored at -80 °C.

Reconstitution of MmTMEM63B-eGFP in liposomes

Purified proteins were incorporated into artificial liposomes, which were formed as previously described.[43,85] A 200 μL 20 mg/mL solution of soy phospholipids (Sigma, 11145) in chloroform was dried in a glass tube under a stream of N_2 while rotating to form a

Please cite this article in press as: Zou et al., TMEM63B functions as a mammalian hyperosmolar sensor for thirst, Neuron (2025), https://doi.org/10.1016/j.neuron.2025.02.012

homogeneous lipid film. Once dry, 5 μL of ddH_2O was added to the bottom of the tube for prehydration followed by 1 mL of 0.4 M sucrose. The solution was incubated for 30 minutes at 50 °C. After the solution cooled to room temperature (21-24 °C), the MmTMEM63B proteins were added to achieve the desired protein-to-lipid ratio, and the protein-lipid solution was shaken gently on an orbital mixer for an additional 3 hours at 4 °C. Giant artificial liposomes were observed in the recording bath following this incubation period. The protein-lipid solution (5-10 μL) was added to the bath buffer used for patch-clamp recordings and waited approximately 10 min for unilamellar blisters to form. For imaging of reconstituted liposomes, a protein-to-lipid ratio of 1:100 (wt:wt) was sufficient. Confocal images of liposomes were obtained using a confocal microscope (IXplore SpinSR, Olympus) with a 100× oil-immersion objective lens and an excitation wavelength of 488 nm.

Isolation and primary culture of SFO neurons

Adult mice were decapitated and the brains were rapidly removed to iced (4℃) Hank's buffer supplemented with antibiotics (100 U/ml penicillin/streptomycin). Under the operating microscope, the SFO was dissected free of surrounding tissue and then placed in DMEM warmed to 37 ℃ containing 0.125% trypsin. Following incubation for 40 min and centrifugation, the cell pellet was resuspended in DMEM, and recentrifuged. The resultant pellet was again resuspended in Neurobasal A media (Gibco) supplemented with antibiotics, plated onto plated onto 10-mm square glass poly-L-lysine coated cell slides placed in 24-well plate in a 5% CO_2 environment at 37 ℃ until the cells attached to the dish. The cells were maintained in the incubator until use (12 h to three days following isolation).

Patch-clamp recording

For the electrophysiological recordings in CHO or HEK293T cells, pCMV-HsTMEM63B-IRES-eGFP construct was transfected into CHO or HEK293T cells using lipofectamine 3000 (Thermo Fisher Scientific) according to the manufacturer's instructions. All plasmids were transfected at a constant concentration of 1000 ng/ml. The full-length coding sequence of human *TMEM63B* (NM_001318792) was amplified from HEK293 cell cDNA. Cells were seeded 24-48 h following transfection onto matrigel-coated coverslips and used for recordings 4-12 h. Whole-cell currents were recorded under a voltage clamp using 3∼5 MΩ borosilicate glass pipettes. For recordings in CHO cells under hyperosmolarity, cells were continuously perfused (∼3 ml/min) at room temperature with isotonic extracellular solutions containing (mM) 140 NaCl, 5 KCl, 2 $MgCl_2 \cdot 6H_2O$, 2 $CaCl_2 \cdot 2H_2O$, 10 HEPES, and 10 D-glucose, pH 7.4, with NaOH (300 mOsm/kg). Additional sucrose was added to increase the extracellular osmolarity without changing the ion concentration. The pipette solution contained (mM) 140 CsCl, 5 EGTA, and 10 HEPES, pH 7.4, with KOH. For recordings in HEK293T cells under hyposmolarity, cells were continuously perfused (∼3 ml/min) at room temperature with isotonic extracellular solutions containing (mM) 130 Na-Gluconate, 5 K-Gluconate, 1 Ca-Gluconate, 10 HEPES, 10 TEA and 10 D-mannitol, pH 7.4, with NaOH (300 mOsm/kg). Mannitol was excluded to decrease the extracellular osmolarity (270 mOsm/kg) without changing the ion concentration. The pipette solution contained (mM) 155 K-Gluconate, 5 EGTA, and 10 HEPES, pH 7.4, with KOH. The osmolarities of all solutions were assessed by a freezing point osmometer (Gonotec, 3000 Basci, Germany). The whole currents were recorded with a Multi-Clamp 700B amplifier and Digidata 1550B digitizer processed by pClamp11.1 software (Molecular Device). Cells with a membrane resistance below 800 MΩ or series resistance above 10 MΩ were discarded. Currents were sampled at 10 kHz and low-pass filtered at 1 kHz. The cells were held at 0 mV before the application of test protocols. The protocol for measuring the hypertonic-activated currents was a 100 ms ramp from -80 to 80 mV every 2 s. Solution changes were performed manually using a 20 mL syringe. The whole-cell currents were recorded in the isotonic solution (300 mOsm/kg) for 2 minutes and then switched to a hyperosmotic solution (320, 350, 400, 500 and 600 mOsm/kg) for 3 minutes before isotonic wash-out.

For the electrophysiological recordings in SFO neurons, wild-type or *Tmem63b*$^{HA\text{-}fl/HA\text{-}fl}$ mice were injected with AAV-CaMK2α-mCherry or AAV-CaMK2α-Cre-mCherry virus in the SFO for at least two weeks. Mice were anesthetized with pentobarbital sodium (50 mg/kg) and then quickly decapitated to remove the brain into ice-cold cutting solution containing (in mM) 2 KCl, 1.25 Na_2HPO_4, 0.2 $CaCl_2$, 12 $MgSO_4$, 10 D-Glucose, 220 Sucrose and 26 $NaHCO_3$ and oxygenated with 95% O_2 + 5% CO_2. Coronal brain slices including the SFO (300 μm) were prepared with a vibratome (VT1200S, Leica). After sectioning, the slices were incubated in standard artificial cerebrospinal fluid (ACSF) containing (in mM) 126 NaCl, 2.5 KCl, 1.25 Na_2HPO_4, 2 $CaCl_2$, 10 D-Glucose, and 26 $NaHCO_3$ were oxygenated with 95% O_2 + 5% CO_2 for 20-30 min at 34 ℃. Then, the slices were allowed to recover for at least 1 h at room temperature before recording. Additional sucrose was added to increase the extracellular osmolarity without changing the ion concentration. For recordings under hyposmolarity, the extracellular solution containing (in mM) 116 NaCl, 2.5 KCl, 1.25 Na_2HPO_4, 2 $CaCl_2$, 10 D-Glucose, and 26 $NaHCO_3$ were utilized. Pipette solutions contain (in mM) 130 K-Gluconate, 20 KCl, 10 HEPES, 0.2 EGTA, 10 NaCreatine, 0.3 Na_2-ATP and 4 Mg-ATP were used in this study. Neurons exhibiting red fluorescence were chosen for recording. Action potentials were cell-attached recorded and when recording glutamate-evoked EPSC, cells were voltage-clamped at -70 mV in ACSF containing 10 μM SR95531 to block $GABA_a$ receptors. Focal responses were evoked by exogenous glutamate applied toward the soma of SFO excitatory neurons via a patch pipette containing 50 μM glutamate with a pressure of 30 psi under the control of pressure application system (LHDA0533115H, The Lee Co., Westbrook, CT, USA). When recording hyperosmotic currents in SFO neurons, cells were voltage-clamped at -70 mV and were recorded in ACSF containing 50 μM APV, 20 μM CNQX and 10 μM SR95531 to block glutamate and $GABA_a$ receptors. Path-clamp recordings were performed using a Multi-Clamp 700B amplifier, with signals being recorded/analyzed using the Digidata 1550B data acquisition system and pClamp 11.2 software package (Molecular Devices).

Please cite this article in press as: Zou et al., TMEM63B functions as a mammalian hyperosmolar sensor for thirst, Neuron (2025), https://doi.org/10.1016/j.neuron.2025.02.012

For the electrophysiological recordings in the MmTMEM63B-reconstituted proteoliposomes, the protocol used to record currents from proteoliposomes was previously reported.[39] A 1:400 protein-to-lipid ratio (wt:wt) was used for current recordings. For the MmTMEM63B-eGFP channel recordings, the bath solutions contained (in mM) 140 KCl, 10 HEPES, 1 $MgCl_2$, 10 glucose, pH 7.3 adjusted with KOH (300 mOsm/kg), and the internal solution contained (in mM) 130 NaCl, 5 KCl, 10 HEPES, 10 TEA-Cl, 1 $CaCl_2$, 1 $MgCl_2$, pH 7.3 adjusted with NaOH. For the hypertonic stimulus (320, 350, 400, 500 and 600 mOsm/kg) to obtain activated channel activity of MmTMEM63B, additional sucrose was added to the pipette buffer. For the blockage of channel activity, 30 μM $GdCl_3$ was added to the pipette buffer. Borosilicate glass pipettes (BF150-86-10, Sutter Instrument) were pulled using a pipette puller (P-97, Sutter Instrument) to a diameter corresponding to the optimal pipette resistance, which was in the range of 4.0-6.0 MΩ. The patch resistance to proteoliposomes increased to more than 1 GΩ. Patch-clamp experiments in liposomes were performed in excised patch (inside-out for liposomes) mode using an EPC-10 amplifier and Patchmaster software (HEKA Electronic, Lambrecht, Germany), filtered at 2 kHz and digitized at 20 kHz. The channel recordings can be analyzed using pCLAMP 11.2 software, and data were plotted using GraphPad Prism 8.0. The current responses in the empty liposomes and MmTMEM63B-reconstituted proteoliposomes were counted under isotonic or hypertonic conditions holding at 40 mV. The integrated current was calculated as the area above baseline for a 10-second duration. All experiments were performed at room temperature.

QUANTIFICATION AND STATISTICAL ANALYSIS

Statistical analysis was performed by IBM SPSS 22.0 or GraphPad Prism 8.0.2. Figures were plotted using GraphPad Prism 8.0.2. Corresponding statistical methods were selected according to different experimental designs and data types. For individual parametric samples, when assumptions of normality and equal variances were met, *Student's unpaired t* tests were used; for normally distributed data with unequal variances, an unpaired two-tailed *Student's unpaired t* tests with *Welch's* correction is applied. For individual nonparametric samples, *Mann-Whitney* tests were conducted. For paired parametric samples, when the assumptions of normal distribution and homoscedasticity are fulfilled for correlated data, a paired Student's *t* test is applied; in cases where these assumptions are not met, we resorted to the *Wilcoxon* matched-pairs signed rank test. *One-way* ANOVA was used for comparisons among multiple groups. The *LSD* method was used for pairwise comparison among multiple groups in the case of homogeneity of variances, while *Dunnett's T3* method was used in the case of uneven variances. Two-way ANOVA test were employed when the response was affected by two factors. Data are presented as the mean ± SEM or mean ± SD. Statistical significance is defined as ns (non-significant), $^{*}p < 0.05$, $^{**}p < 0.01$, $^{***}p < 0.001$. The Statistical details of experiments are shown in the figure legends, including the statistical tests used, exact value of n, what n represents, the definition of center, and dispersion and precision measures. All the statistical details of experiments can be found in the figure legends.

Neuron, Volume *113*

Supplemental information

TMEM63B functions as a mammalian hyperosmolar sensor for thirst

Wenjie Zou, Siqi Deng, Xingyu Chen, Jiamin Ruan, Huize Wang, Wuqiang Zhan, Jingxin Wang, Zhiyong Liu, and Zhiqiang Yan

Figure S1

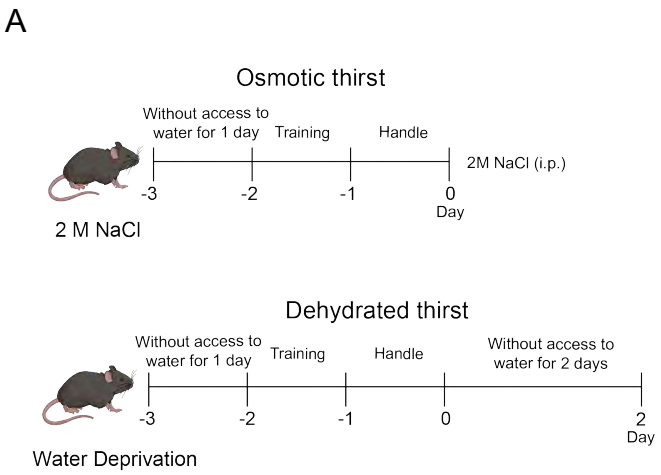
A
Osmotic thirst
Without access to water for 1 day
Training
Handle
2M NaCl (i.p.)
-3
-2
-1
0
Day
2 M NaCl
Dehydrated thirst
Without access to water for 1 day
Training
Handle
Without access to water for 2 days
-3
-2
-1
0
2
Day
Water Deprivation
B
Plasma osmolarity (mOsm/kg)
400
380
360
340
320
300
***
***
Control
2 M NaCl
Water deprivation

Figure S1. The generation of osmotic thirst and water deprivation thirst model, related to Figure 1.

(A) Schematic diagram and experimental procedures of the osmotic or dehydrated thirst model. i.p., intraperitoneal injection.

(B) Plasma osmolality in wild type mice under osmotic thirst and water deprivation shown in **(A)** (Mean ± SEM, ***$P < 0.001$, *Student's unpaired t* test, n = 9, n represents the number of mice).

Figure S2

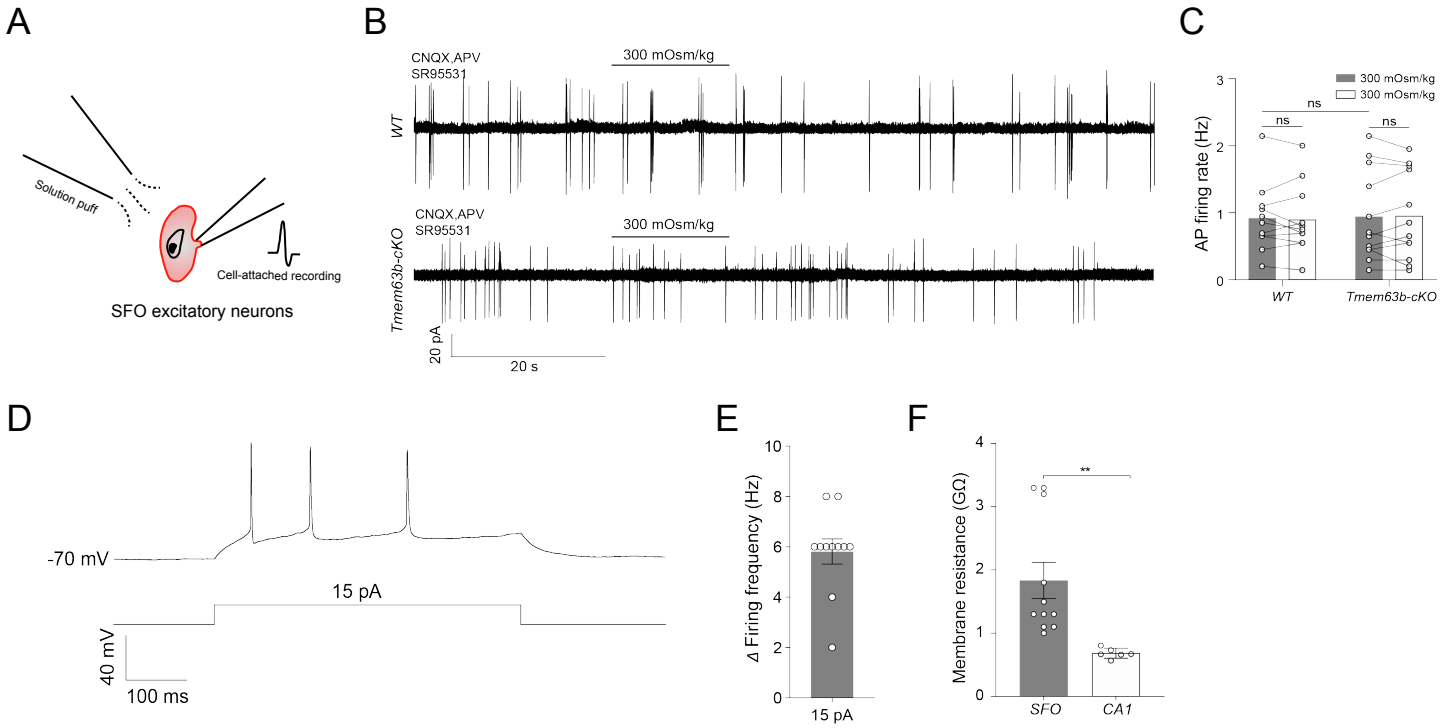
A
Solution puff
Cell-attached recording
SFO excitatory neurons
B
CNQX,APV
SR95531
300 mOsm/kg
WT
CNQX,APV
SR95531
300 mOsm/kg
Tmem63b-cKO
20 pA
20 s
C
300 mOsm/kg
300 mOsm/kg
ns
ns
ns
AP firing rate (Hz)
WT
Tmem63b-cKO
D
-70 mV
15 pA
40 mV
100 ms
E
Δ Firing frequency (Hz)
15 pA
F
**
Membrane resistance (GΩ)
SFO
CA1

Figure S2. Action potential firing and whole-cell current of SFO excitatory neurons under isotonic stimulus or current injection, related to Figure 1 and Figure 2.

(A) Schematic diagram showing hyperosmotic solution puffing applied on the SFO excitatory neurons.

(B) Representative traces of action potential (AP) firing of SFO excitatory neurons in wild-type or *Tmem63b* cKO mice. Isotonic puffing (300 mOsm/kg) for 15 s was applied.

(C) The firing rate of SFO excitatory neurons of WT or *Tmem63b*-cKO mice show no significant change over time in isotonic solution (300 mOsm/kg). n.s., no significant difference, *Student's paired* and *unpaired t-test*, *n* = 11-12. n represents the number of SFO excitatory neurons.

(D) Representative trace of spike firing in SFO excitatory neurons induced by injection of 15-pA current.

(E) Quantification of number of action potential firing shown in **(D)** (n = 11). n represents the number of SFO excitatory neurons.

(F) Measurement on SFO membrane resistance showed that SFO neurons have a high membrane resistance, compared with that of CA1 neurons (Mean ± SEM, $^{**}P < 0.01$, *Student's unpaired t* test, n = 11 for SFO group, n = 6 for CA1 group). n represents the number of neurons.

Figure S3

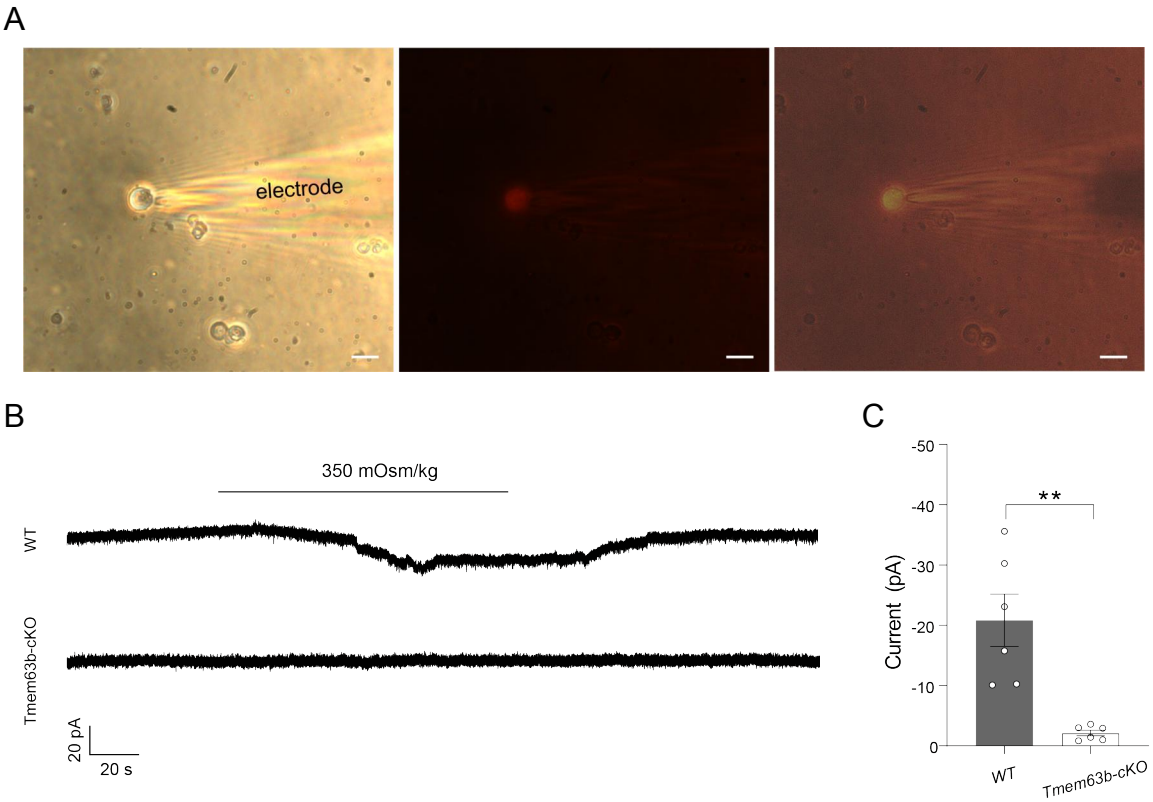
A
electrode
B
350 mOsm/kg
WT
Tmem63b-cKO
20 pA
20 s
C
Current (pA)
-50
-40
-30
-20
-10
0
**
WT
Tmem63b-cKO

Figure S3. Hyperosmotic stimulus can induce inward current in isolated SFO excitatory neurons directly, which is TMEM63B-dependent, related to Figure 1 and Figure 2.

(A) Representative images showing one SFO excitatory neuron labeled by AAV virus expressed with red fluorescence. Scale bar: 20 μm.

(B) Representative traces showing inward current induced by 350 mOsm/kg in isolated SFO excitatory neuron, which is lost in *Tmem63b*-knockout group.

(C) Quantification of current amplitude shown in **(B)**. Mean ± SEM, $^{**}P < 0.01$, *Student's unpaired t* test, n = 6 each, n represents the number neurons.

Figure S4

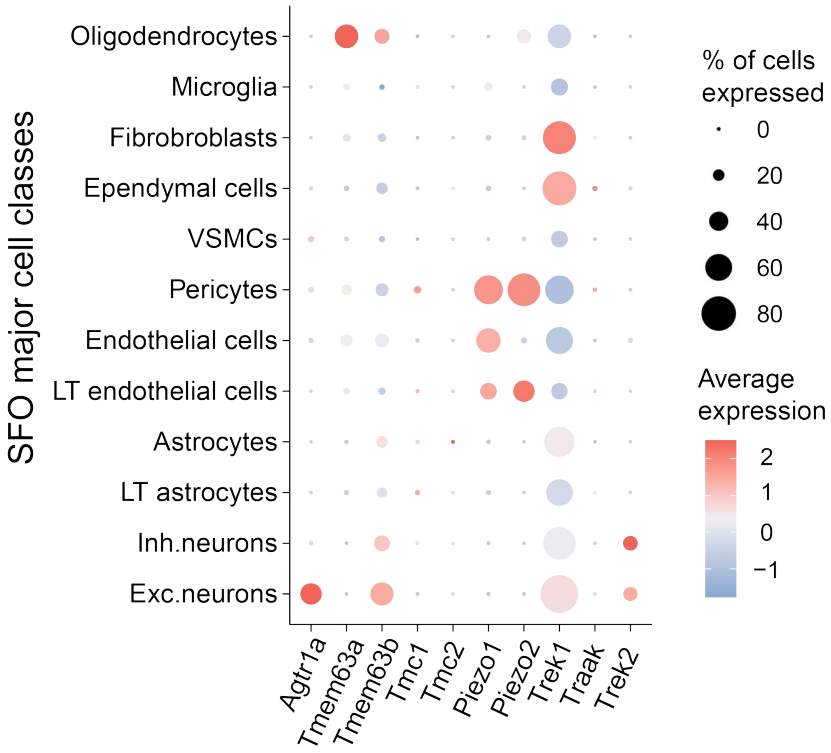
SFO major cell classes
Oligodendrocytes
Microglia
Fibrobroblasts
Ependymal cells
VSMCs
Pericytes
Endothelial cells
LT endothelial cells
Astrocytes
LT astrocytes
Inh.neurons
Exc.neurons
Agtr1a
Tmem63a
Tmem63b
Tmc1
Tmc2
Piezo1
Piezo2
Trek1
Traak
Trek2
% of cells expressed
0
20
40
60
80
Average expression
2
1
0
−1

Figure S4. scRNA-Seq analysis of osmosensitive or mechanosensitive ion channel expression in the SFO, related to Figure 2.

Dot plot of cell-type-specific expression for osmosensitive or mechanosensitive ion channels expression in the major cell classes of the SFO based on the published data [S1]. Dot size is proportional to % of cells with transcript count > 0 expression, color scale represents Z scored average gene expression, n = 7950 cells.

Figure S5

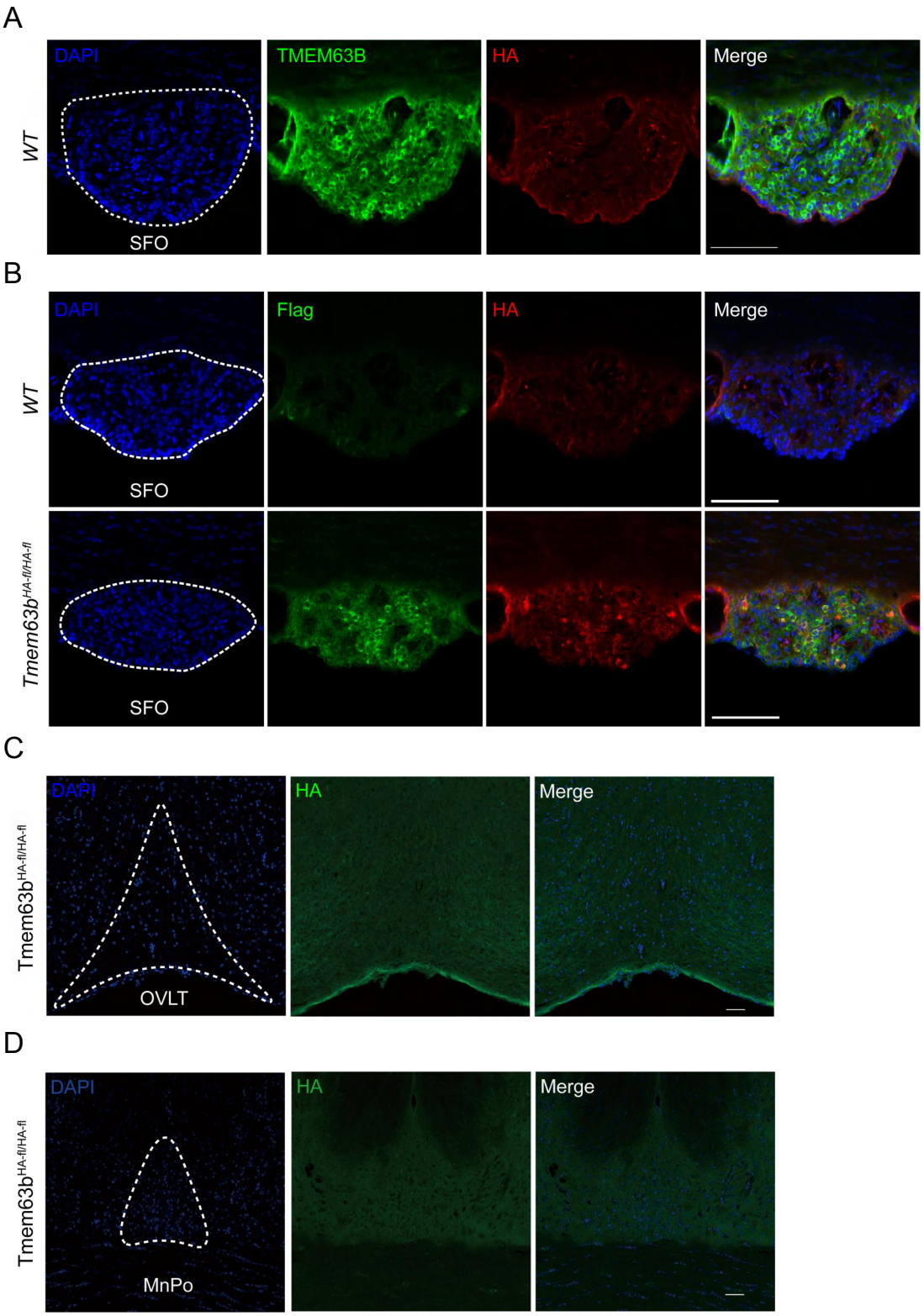
A
DAPI
TMEM63B
HA
Merge
WT
SFO
B
DAPI
Flag
HA
Merge
WT
SFO
Tmem63b HA-fl/HA-fl
SFO
C
DAPI
HA
Merge
Tmem63b HA-fl/HA-fl
OVLT
D
DAPI
HA
Merge
Tmem63b HA-fl/HA-fl
MnPo

Figure S5. Protein expression patterns of TMEM63B in SFO, OVLT and MnPO, related to Figure 2.

(A) Representative images show the expression of endogenous TMEM63B detected by anti-HA antibody and custom-made TMEM63B polyclonal antibody in the SFO of *WT* mice. Scale bar 100 μm.

(B) Representative images show the expression of endogenous TMEM63B in the SFO of *WT* and *Tmem63b*$^{HA\text{-}fl/HA\text{-}fl}$ mice, stained with antibodies against a fusion HA (red) or 3×Flag (green) tag. WT mice show no signal in the SFO with these two antibodies (Upper panel). Scale bar 100 μm.

(C) Representative images show no expression of endogenous TMEM63B in the OVLT of *Tmem63b*$^{HA\text{-}fl/HA\text{-}fl}$ mice, stained with antibody against a fusion HA (Green). Scale bar 100 μm.

(D) Representative images show that the expression of endogenous TMEM63B in the MnPO of *Tmem63b*$^{HA\text{-}fl/HA\text{-}fl}$ mice was barely detected. Scale bar 100 μm.

Figure S6

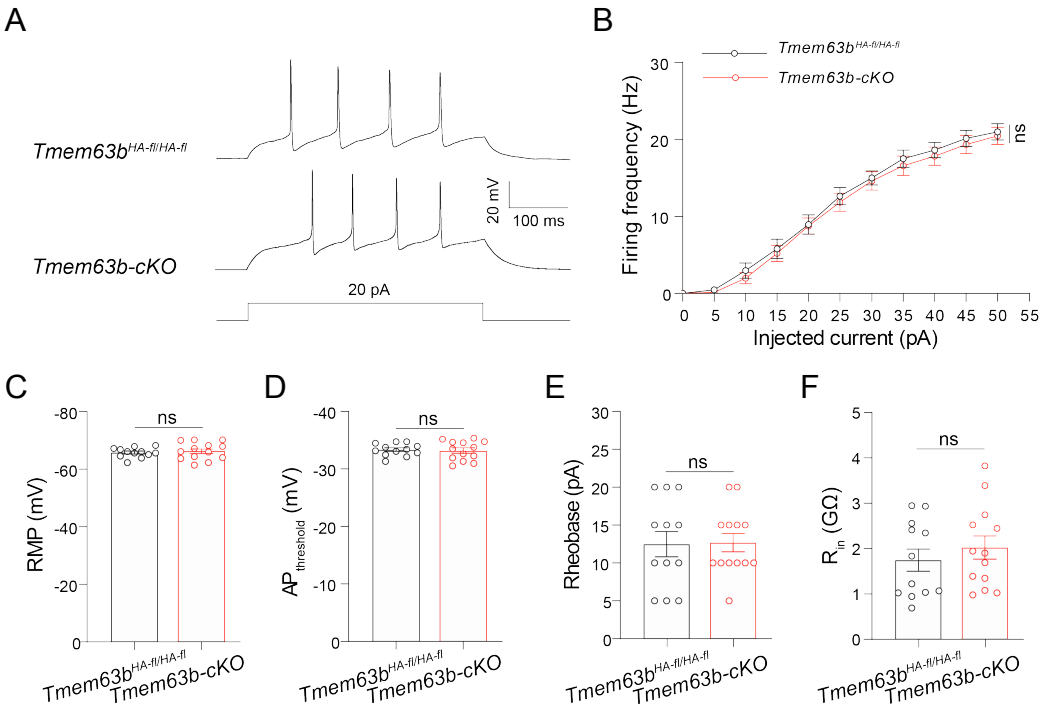
A
Tmem63b^HA-fl/HA-fl
Tmem63b-cKO
20 mV
100 ms
20 pA
B
Tmem63b^HA-fl/HA-fl
Tmem63b-cKO
Firing frequency (Hz)
Injected current (pA)
ns
C
RMP (mV)
ns
Tmem63b^HA-fl/HA-fl
Tmem63b-cKO
D
AP threshold (mV)
ns
Tmem63b^HA-fl/HA-fl
Tmem63b-cKO
E
Rheobase (pA)
ns
Tmem63b^HA-fl/HA-fl
Tmem63b-cKO
F
R_in (GΩ)
ns
Tmem63b^HA-fl/HA-fl
Tmem63b-cKO

Figure S6. Basic intrinsic properties of TMEM63B-deficient SFO excitatory neurons do not show significant differences, related to Figure 2.

(A) Representative current-clamp recordings and **(B)** Summary input-output curves from SFO excitatory neurons of control (n = 12) and *Tmem63b* cKO (n = 13) mice show similar AP firing in response to current injections. Statistics were presented as mean ± SEM and analyzed by *Two-way ANOVA*.

(C-F) Summary data of resting membrane potential (RMP) **(C)**, AP threshold **(D)**, rheobase current **(E)** and membrane input resistance **(F)** of control (n = 12) and *Tmem63b* cKO (n = 13) SFO excitatory neurons. Statistics were analyzed by *Student's unpaired t* test. 5-weeks WT or *Tmem63b-cKO* mice were used for all experiments.

n represents the number of neurons.

Figure S7

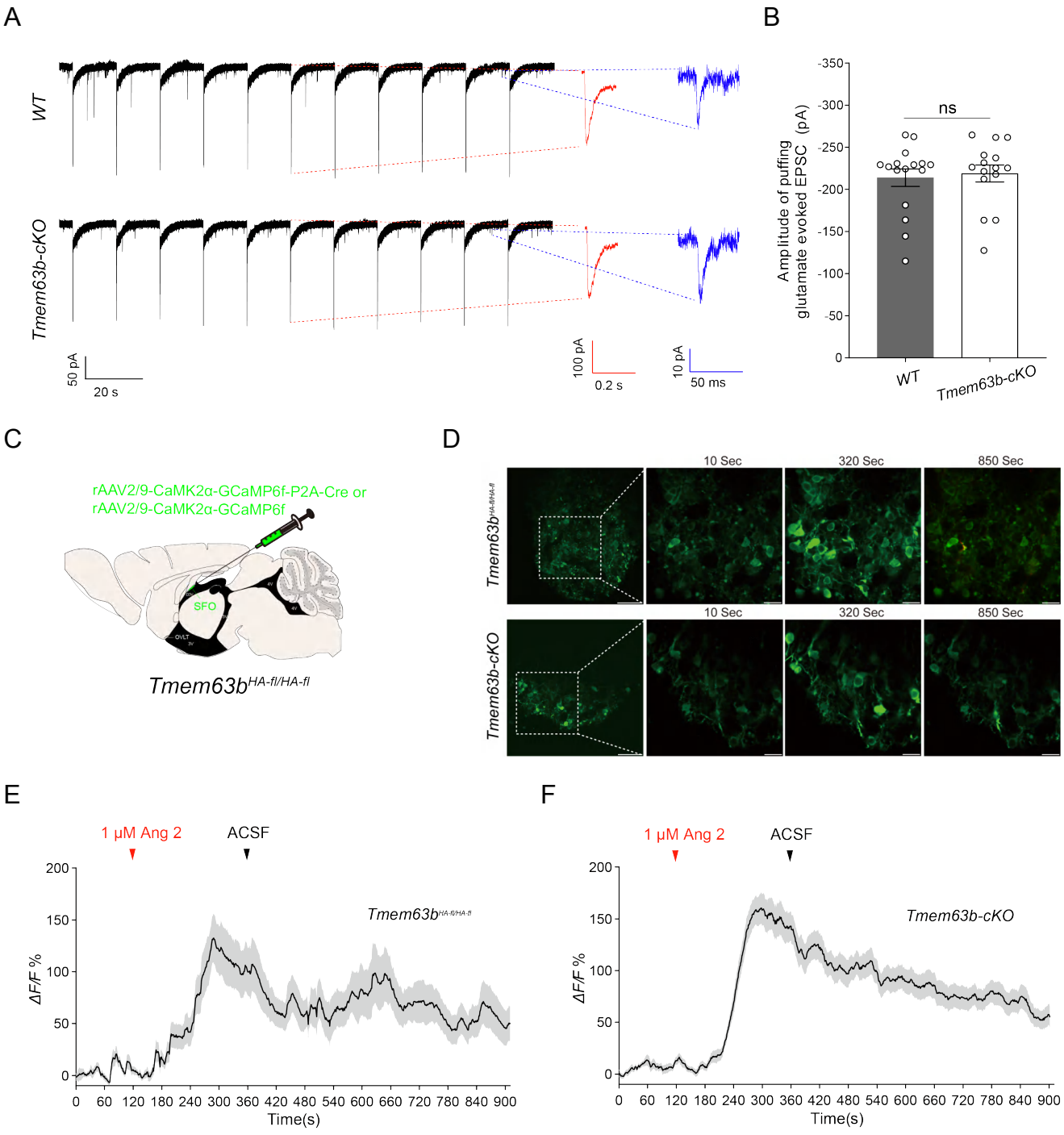
A
WT
Tmem63b-cKO
50 pA
20 s
100 pA
0.2 s
10 pA
50 ms
B
Amplitude of puffing glutamate evoked EPSC (pA)
-350
-300
-250
-200
-150
-100
-50
0
ns
WT
Tmem63b-cKO
C
rAAV2/9-CaMK2α-GCaMP6f-P2A-Cre or
rAAV2/9-CaMK2α-GCaMP6f
SFO
OVLT
3V
Tmem63b HA-fl/HA-fl
D
10 Sec
320 Sec
850 Sec
Tmem63b HA-fl/HA-fl
Tmem63b-cKO
E
1 μM Ang 2
ACSF
Tmem63b HA-fl/HA-fl
ΔF/F %
200
150
100
50
0
0 60 120 180 240 300 360 420 480 540 600 660 720 780 840 900
Time(s)
F
1 μM Ang 2
ACSF
Tmem63b-cKO
ΔF/F %
200
150
100
50
0
0 60 120 180 240 300 360 420 480 540 600 660 720 780 840 900
Time(s)

Figure S7. TMEM63B-deficient SFO excitatory neurons show similar responses with wild type to non-osmolarity stimulation, related to Figure 2.

(A) Representative excitatory postsynaptic currents (EPSC) induced by puffing 50 μM glutamate 30 ms in every 15 s in the SFO excitatory neurons of control and *Tmem63b-cKO* mice. Comparison between puffing-glutamate evoked EPSC (red, scale bar: 100 pA, 0.2 s) and the spontaneous EPSC (blue, scale bar: 10 pA, 50 ms) is displayed.

(B) Quantification of amplitude of glutamate evoked EPSC. All error bars denote the mean ± SEM, n = 15-16, *Student's unpaired t* test, n represents the number of neurons.

(C) Schematic diagram of injecting rAAV2/9-CaMK2α-GCaMP6f or rAAV2/9-CaMK2α-GCaMP6f-Cre in the SFO to expression GCaMP6f in SFO excitatory neurons in *Tmem63b*$^{HA\text{-}fl/HA\text{-}fl}$ mice.

(D) Representative images showing SFO excitatory neurons calcium activity before, during and after bath application of 1 μM AngII in control and *Tmem63b-cKO* mice. Scale bar: wide-field view 50 μm, local view at different time point 20 μm.

(E-F) Similar calcium fluorescence intensity in SFO excitatory neurons in control and *Tmem63b-cKO* mice in response to 1 μM AngII application. All error bars denote the mean ± SEM, n = 34-39, n represents the number of neurons.

Figure S8

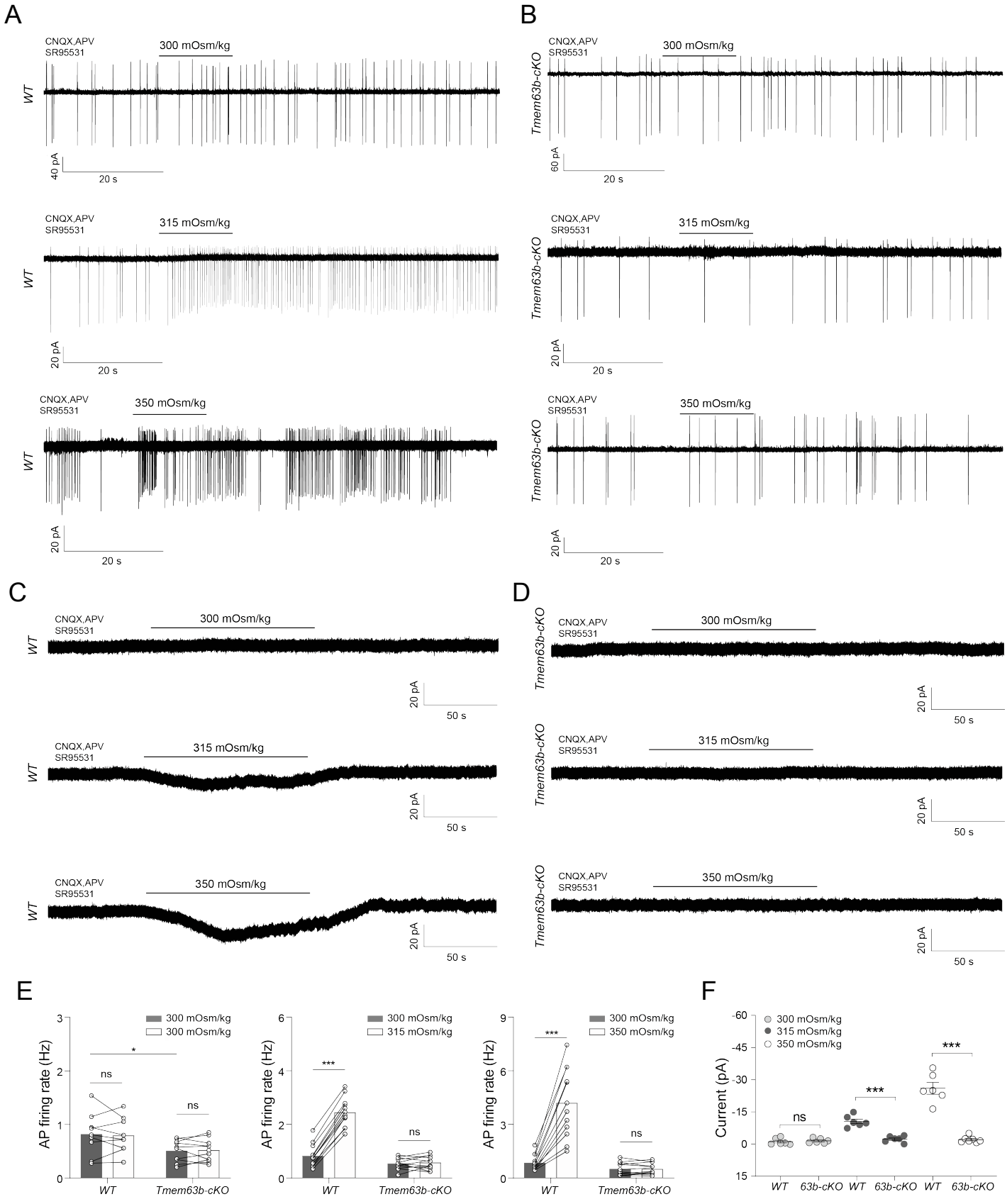
A
B
C
D
E
F
CNQX,APV
SR95531
300 mOsm/kg
315 mOsm/kg
350 mOsm/kg
WT
Tmem63b-cKO
40 pA
60 pA
20 pA
50 pA
20 s
50 s
AP firing rate (Hz)
ns
*
***
Current (pA)
63b-cKO

Figure S8 TMEM63B is required for mediating the hyperosmosensitive response in SFO excitatory neurons from older mice aged 12-week, related to Figure 1 and Figure 2.

(A-B) Representative traces of AP firing of SFO excitatory neurons in control **(A)** and *Tmem63b*-cKO mice **(B)** under 15-s puffing of hyperosmotic solution at 300 mOsm/kg (top), 315 mOsm/kg (middle) or 350 mOsm/kg (bottom). In all the recordings above, the basal AP firing rate of SFO excitatory neurons were first recorded for 20 s and the neurons were exposed to a brief 15-second puff of solution that varied in osmolarity.

(C-D) Representative traces of current recorded in control **(C)** or TMEM63B-deficient **(D)** SFO excitatory neurons in response to isotonic and hypertonic stimuli of 300 mOsm/kg (top), 315 mOsm/kg (middle) or 350 mOsm/kg (bottom). After recording in isotonic solution for 1 min, hypertonic perfusion was applied to SFO excitatory neurons for 2 min, followed by an isotonic washout.

(E) The AP firing rate of SFO excitatory neurons in WT mice shows a reversible increase in response to 315 mOsm/kg (middle, n = 12) or 350 mOsm/kg (right, n = 12) hypertonic stimulus, which was lost in *Tmem63b*-cKO mice. The AP firing rate of SFO excitatory neurons in control or *Tmem63b*-cKO mice remained unchanged in response to isotonic solution puff (300 mOsm/kg, left, n = 9-10). The spontaneous firing rate of *Tmem63b*-cKO SFO excitatory neurons was lower than that in control mice. Statistics were analyzed by *Student's paired t* test. n represents the number of neurons recorded in each experiment.

(F) Hyperosmosensitive currents induced by 315 mOsm/kg (middle) or 350 mOsm/kg (right) were eliminated in *Tmem63b*-cKO mice. No current response was observed under isotonic perfusion (left), n = 6-7. Statistics were analyzed by *Student's unpaired t* test, n represents the number of neurons recorded in each experiment.

Figure S9

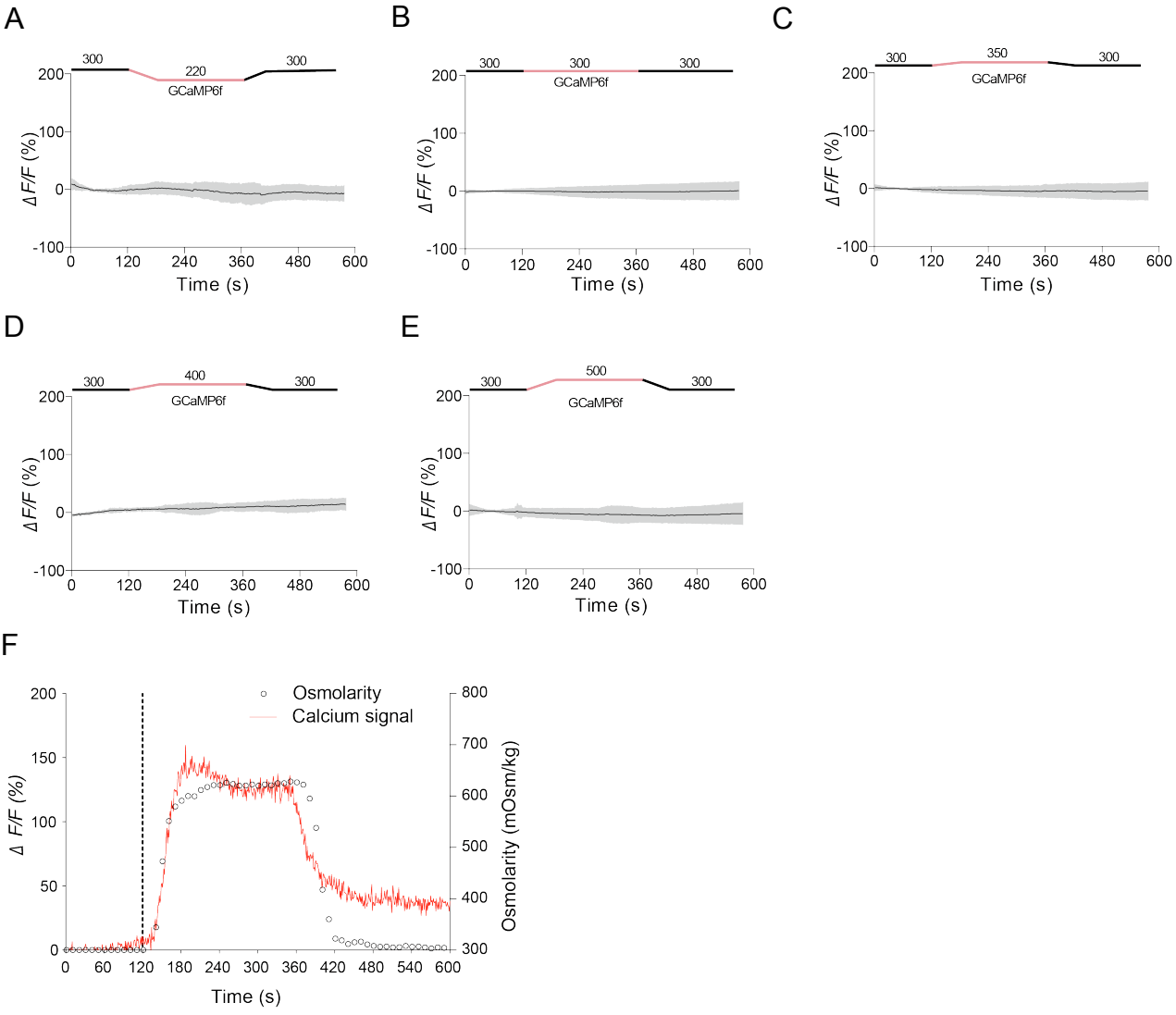
A
300
220
300
GCaMP6f
ΔF/F (%)
Time (s)
B
300
300
300
GCaMP6f
ΔF/F (%)
Time (s)
C
300
350
300
GCaMP6f
ΔF/F (%)
Time (s)
D
300
400
300
GCaMP6f
ΔF/F (%)
Time (s)
E
300
500
300
GCaMP6f
ΔF/F (%)
Time (s)
F
Osmolarity
Calcium signal
Δ F/F (%)
Osmolarity (mOsm/kg)
Time (s)

Figure S9. N2a cells transfected with GCaMP6f showed no significant calcium responses to osmolarity changes, related to Figure 3.

(A-E) The calcium fluorescence intensity of N2a cells transfected with GCaMP6f, in response to hyposmolarity of 220 mOsm/kg **(A)**, isotonic solution **(B)** and hyperosmolarity of 350 mOsm/kg **(C)**, 400 mOsm/kg **(D)**, 500 mOsm/kg **(E)**. The red line indicates the hyperosmotic stimulus for 4 minutes. The grey shadow denotes the mean ± SD, n = 44-199, n represents the number of cells.

(F) The calcium response in TMEM63B transfected N2a cells coincides with the osmolarity changes. Calcium signal (red line) responses with osmolarity change (black dot) in a N2a cell expressing TMEM63B. The calcium signal was captured for 10 minutes at 0.5 Hz and the osmolarity of the external solution was measured every 10 seconds. The dashed line indicates the onset time of application of the hypertonic solution. The left y-axis shows the response of calcium signaling ($\Delta F/F$), and the right y-axis represents the osmolarity of the external solution (mOsm/kg).

Figure S10

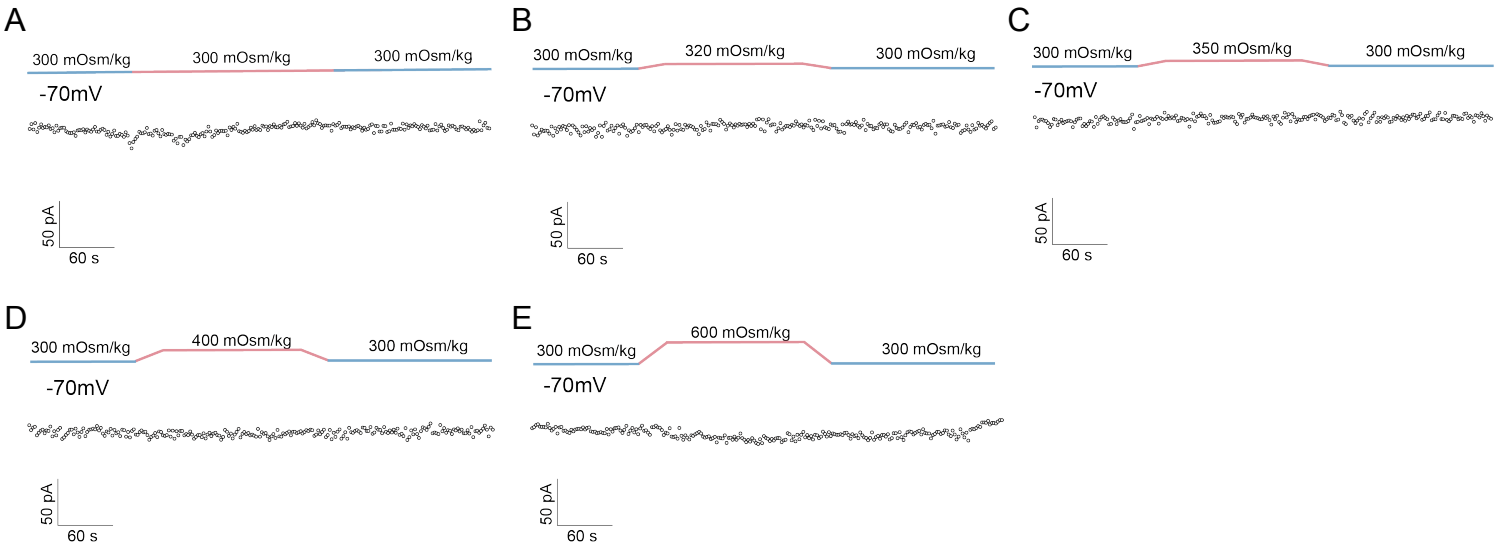
A
300 mOsm/kg
300 mOsm/kg
300 mOsm/kg
-70mV
50 pA
60 s
B
300 mOsm/kg
320 mOsm/kg
300 mOsm/kg
-70mV
50 pA
60 s
C
300 mOsm/kg
350 mOsm/kg
300 mOsm/kg
-70mV
50 pA
60 s
D
300 mOsm/kg
400 mOsm/kg
300 mOsm/kg
-70mV
50 pA
60 s
E
300 mOsm/kg
600 mOsm/kg
300 mOsm/kg
-70mV
50 pA
60 s

Figure S10. Untransfected CHO cells showed no significant hyperosmosensitive currents, related to Figure 4.

(A-E) Representative whole-cell currents in untransfected CHO cells were recorded every two seconds by ramp protocols in 2-min isotonic solution (300 mOsm/kg; blue) followed by 3-min (red) of isotonic solution **(A)** or hypertonic solution of 320 mOsm/kg **(B)**, 350 mOsm/kg **(C)**, 400 mOsm/kg **(D)** and 600 mOsm/kg **(E)**, before isotonic wash-out. Currents at -70 mV over time were plotted.

Figure S11

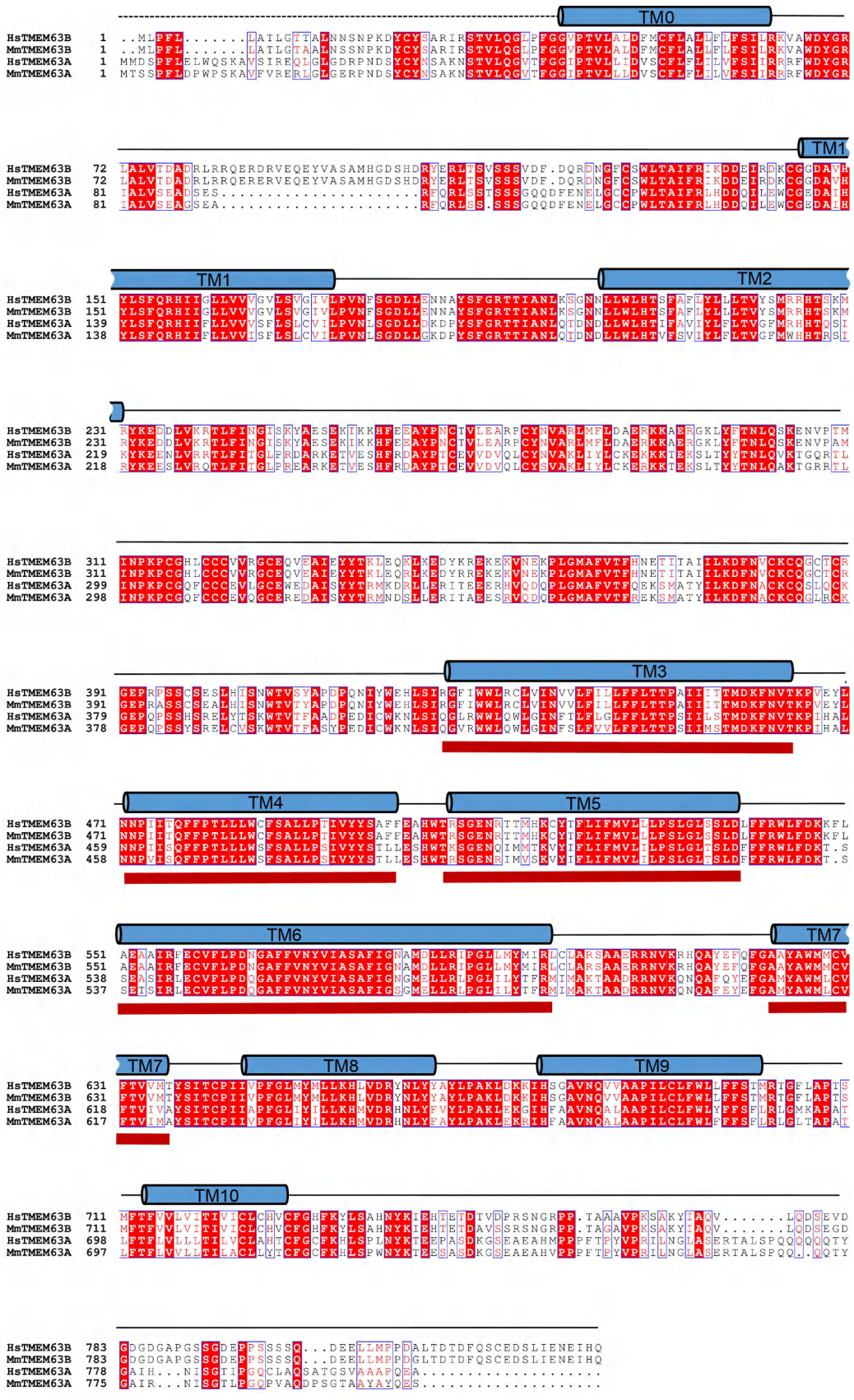
TM0
TM1
TM1
TM2
TM3
TM4
TM5
TM6
TM7
TM7
TM8
TM9
TM10
HsTMEM63B
MmTMEM63B
HsTMEM63A
MmTMEM63A

Figure S11. Alignment of amino acid sequences between human and mouse TMEM63 family proteins based on the model generated by SWISS-MODEL, related to Figure 5.

The transmembrane regions are noted as blue cylinders, and identical residues are colored red, while similar residues are marked in red font. The red lines at the bottom of the sequences indicate the transmembrane helix around the putative pore region of HsTMEM63B, corresponding to the sequence of 426-460, 470-502, 506-539, 550-584, and 622-637.

Figure S12

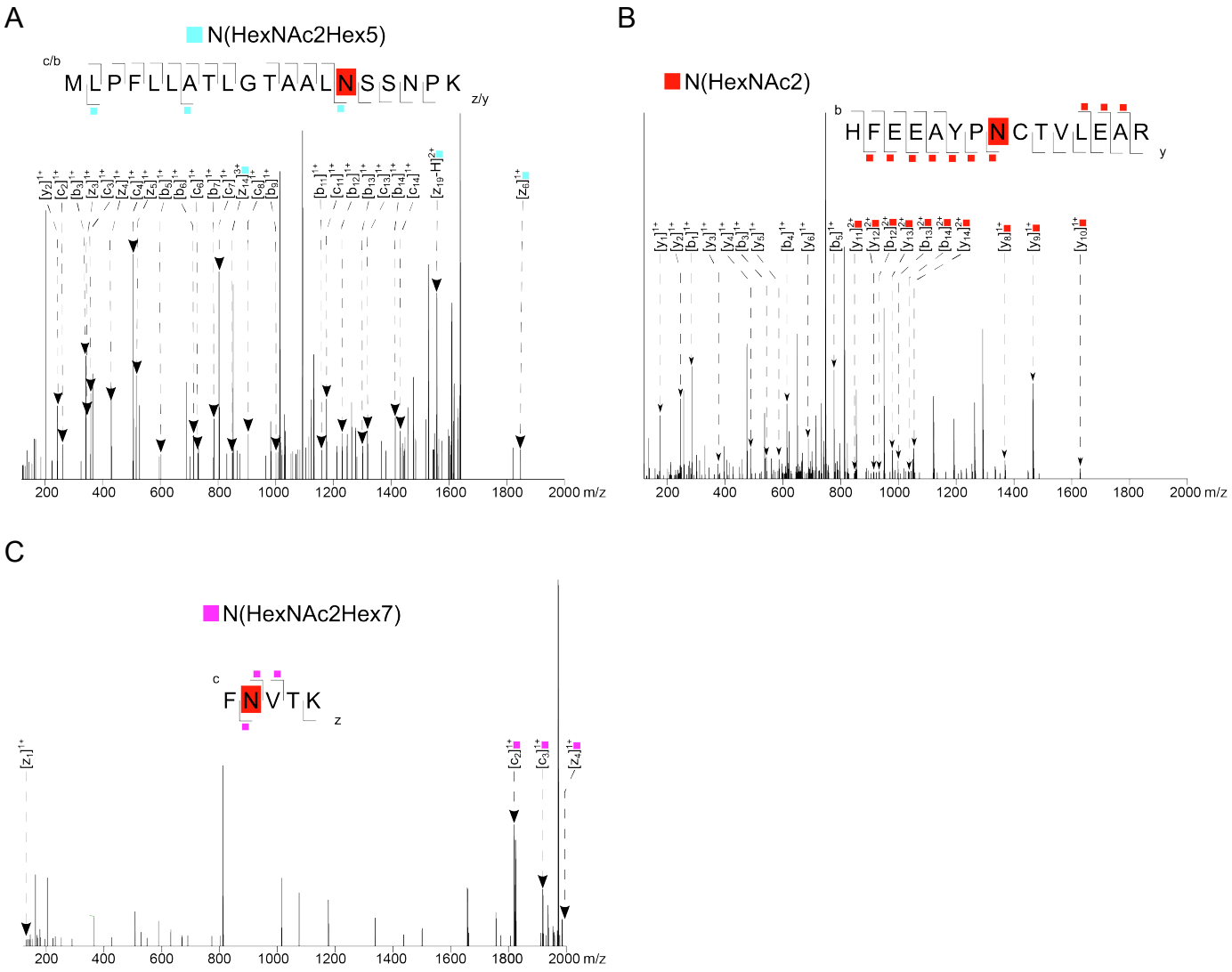
A
N(HexNAc2Hex5)
c/b
M L P F L L A T L G T A A L N S S N P K
z/y
200 400 600 800 1000 1200 1400 1600 1800 2000 m/z
B
N(HexNAc2)
b
H F E E A Y P N C T V L E A R
y
200 400 600 800 1000 1200 1400 1600 1800 2000 m/z
C
N(HexNAc2Hex7)
c
F N V T K
z
200 400 600 800 1000 1200 1400 1600 1800 2000 m/z

Figure S12. Mass spectrometry analysis of the glycosylation sites of MmTMEM63B, related to Figure 5.

(A) The peptide sequence (MLPFLLATLGTAALNSSNPK) at position N15 featured the N-glycosylated oligosaccharide HexNAc2Hex5 (high-mannose N-linked glycan).

(B) The peptide sequence (HFEEAYPNTVLEAR) at position N266 also presented the N-glycosylated oligosaccharide HexNAc2 (complex-type N-linked glycan).

(C) The peptide sequence (FNVTK) at position N462 possessed the N-glycosylated oligosaccharide HexNAc2Hex7 (high-mannose N-linked glycan). By analysis of the mass spectrometry results based on the database, these glycan types were identified.

Figure S13

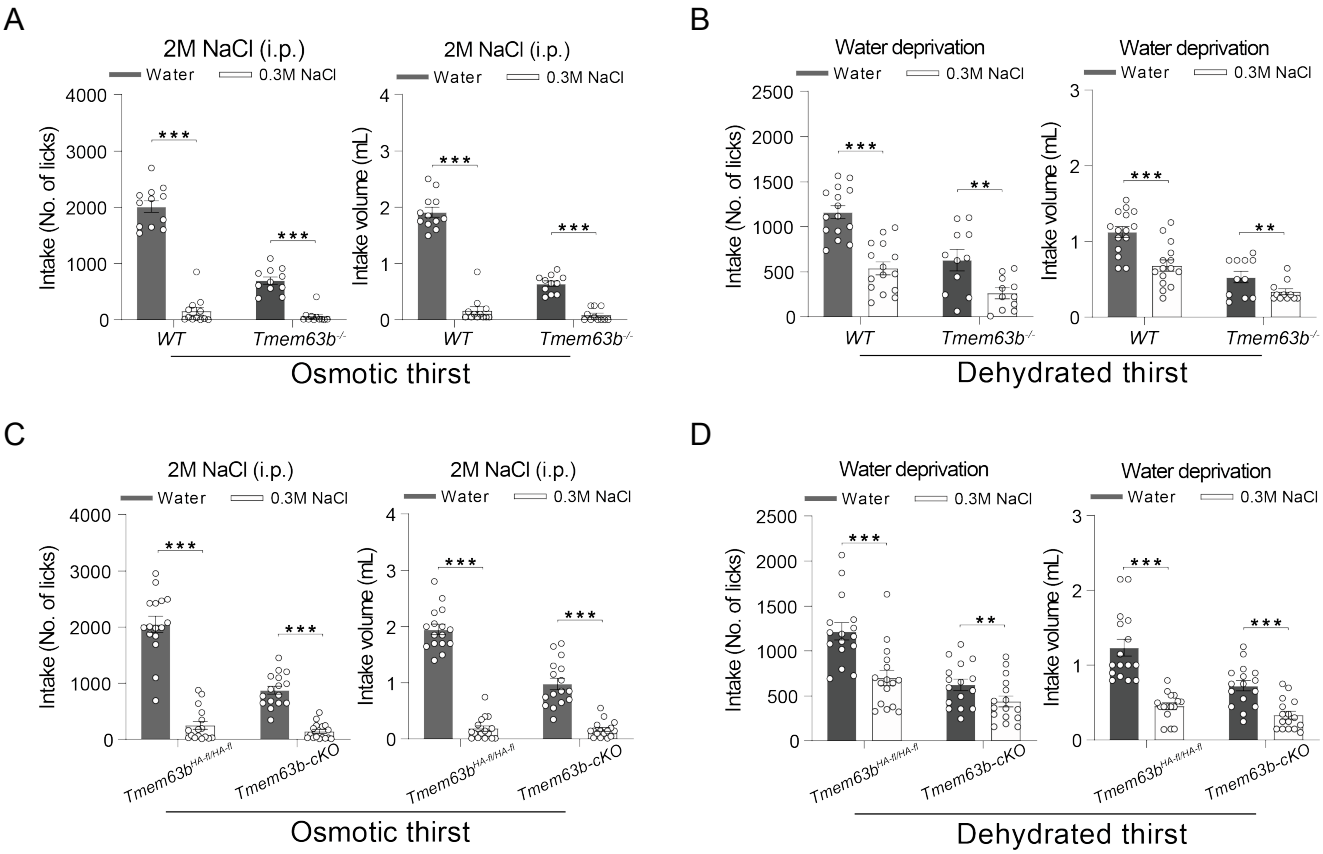
A
2M NaCl (i.p.)
Water
0.3M NaCl
Intake (No. of licks)
Intake volume (mL)
WT
Tmem63b-/-
Osmotic thirst
B
Water deprivation
Dehydrated thirst
C
Tmem63bHA-fl/HA-fl
Tmem63b-cKO
D

Figure S13. Water and hypertonic saline (0.3 M NaCl) intake of *Tmem63b-KO* and *Tmem63b-cKO* mice under osmotic and dehydrated thirst, related to Figure 7.

(A) Water (red) and hypertonic saline intake (0.3 M NaCl, blue) of wild-type and *Tmem63b*$^{-/-}$ mice during a 1-h session after 2 M NaCl injection. Both WT and KO mice showed a strong preference for water, with little hypertonic saline intake under osmotic thirst (n = 11-12).

(B) Water and hypertonic saline intake of wild-type and *Tmem63b* knockout mice after water deprivation during a 1-h session (n = 11-15).

(C) Water and hypertonic saline intake of *Tmem63b*$^{HA\text{-}fl/HA\text{-}fl}$ mice and *Tmem63b*$^{HA\text{-}fl/HA\text{-}fl}$ mice injected with AAV-CaMK2α-Cre-mCherry virus under osmotic thirst during a 1-h session. Both *Tmem63b*$^{HA\text{-}fl/HA\text{-}fl}$ and *Tmem63b-cKO* mice show high water preference and barely consume 0.3 M NaCl (n = 16).

(D) Water and hypertonic saline intake of *Tmem63b*$^{HA\text{-}fl/HA\text{-}fl}$ mice and *Tmem63b*$^{HA\text{-}fl/HA\text{-}fl}$ mice injected with AAV-CaMK2α-Cre-mCherry virus under water deprivation during a 1-h session (n = 16). In these figures above, water or 0.3 M NaCl intake are quantified by two parameters, number of licks (left) and water intake volume (right) during a 1-h session.

All error bars denote the mean ± SEM，***P < 0.001, *Student's unpaired t* test, n represents the number of mice.

The water intake of wild-type, *Tmem63b*$^{-/-}$, *Tmem63b*$^{HA\text{-}fl/HA\text{-}fl}$ and *Tmem63b-cKO* in **(A-D)** were same group of data from Figure 7 **(C-F)**.

Figure S14

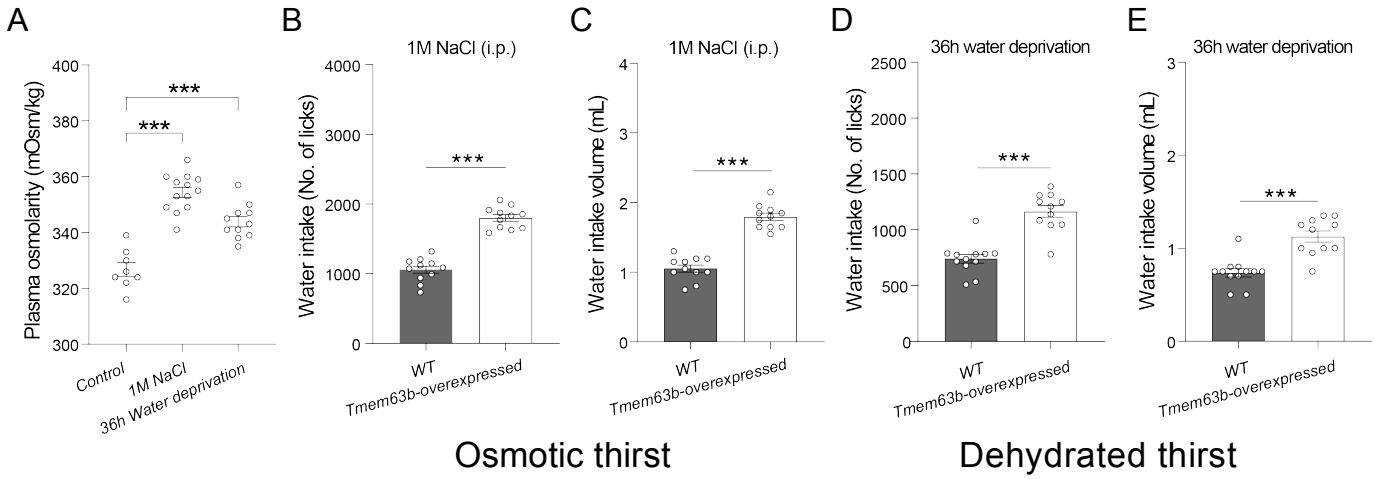
A
B
C
D
E
Plasma osmolarity (mOsm/kg)
400
380
360
340
320
300
***
***
Control
1M NaCl
36h Water deprivation
1M NaCl (i.p.)
Water intake (No. of licks)
4000
3000
2000
1000
0
***
WT
Tmem63b-overexpressed
1M NaCl (i.p.)
Water intake volume (mL)
4
3
2
1
0
***
WT
Tmem63b-overexpressed
36h water deprivation
Water intake (No. of licks)
2500
2000
1500
1000
500
0
***
WT
Tmem63b-overexpressed
36h water deprivation
Water intake volume (mL)
3
2
1
0
***
WT
Tmem63b-overexpressed
Osmotic thirst
Dehydrated thirst

Figure S14. Two-bottle test in moderate osmotic-thirst or dehydrated mice with TMEM63B overexpression in SFO excitatory neuron showed higher water intake than WT mice, related to Figure 7.

(A) Plasma osmolarity in moderate osmotic thirst model and dehydration model (n = 8-13).

(B-C) The water intake of WT or Tmem63b-overexpressed mice under moderate osmotic thirst during a 1-h session (n = 11).

(D-E) The water intake of WT or Tmem63b-overexpressed mice (n = 11-12) under moderate dehydrated thirst during a 1-h session.

Statistics were analyzed by *Student's unpaired t* test, n represents the number of mice.

Figure S15

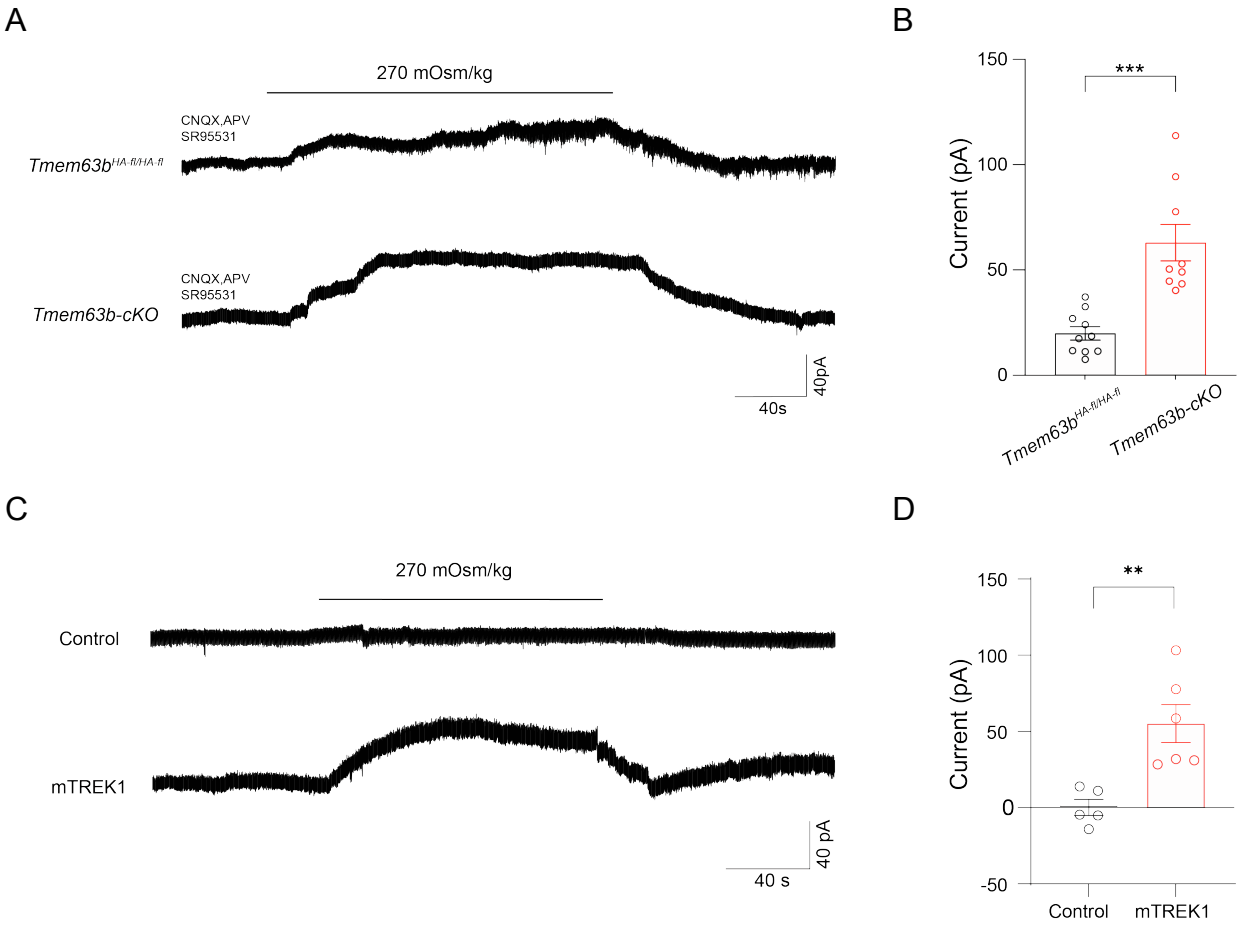
A
270 mOsm/kg
CNQX,APV
SR95531
Tmem63b HA-fl/HA-fl
CNQX,APV
SR95531
Tmem63b-cKO
40pA
40s
B
***
Current (pA)
150
100
50
0
Tmem63b HA-fl/HA-fl
Tmem63b-cKO
C
270 mOsm/kg
Control
mTREK1
40 pA
40 s
D
**
Current (pA)
150
100
50
0
-50
Control
mTREK1

Figure S15. Hypoosmosensitive outwards current recorded in SFO excitatory neuron and the hypoosmosensitive current of heterologously expressed TREK1 in HEK293 under 270 mOsm/kg, related to Figure 4.

(A) Representative trace of outward current in SFO excitatory neuron under hypotonic stimulation, with -50 mV holding.

(B) The amplitude of hyposmolarity-induced outward current was higher in *Tmem63b* knockout SFO excitatory neurons, compared with that in control group (n=9-10, n represents the number of neurons, mean ± SEM, *Student's unpaired t* test, ***$P < 0.001$).

(C) Representative trace for current recording in mouse-TREK1-expressing HEK293T cell or untransfected cell under hypotonic stimulation, with -50 mV holding.

(D) Heterologously expressed TREK1 displayed hypotonic stimulation-induced outward current. Chloride-free solution were applied in the electrophysiological recording to eliminate the effect by the swelling-activated chloride channel SWELL1, expressed endogenously in HEK293T cells (n = 5-6, n represents the number of cells, mean ± SEM, *Student's unpaired t* test, **$P < 0.01$).

Figure S16

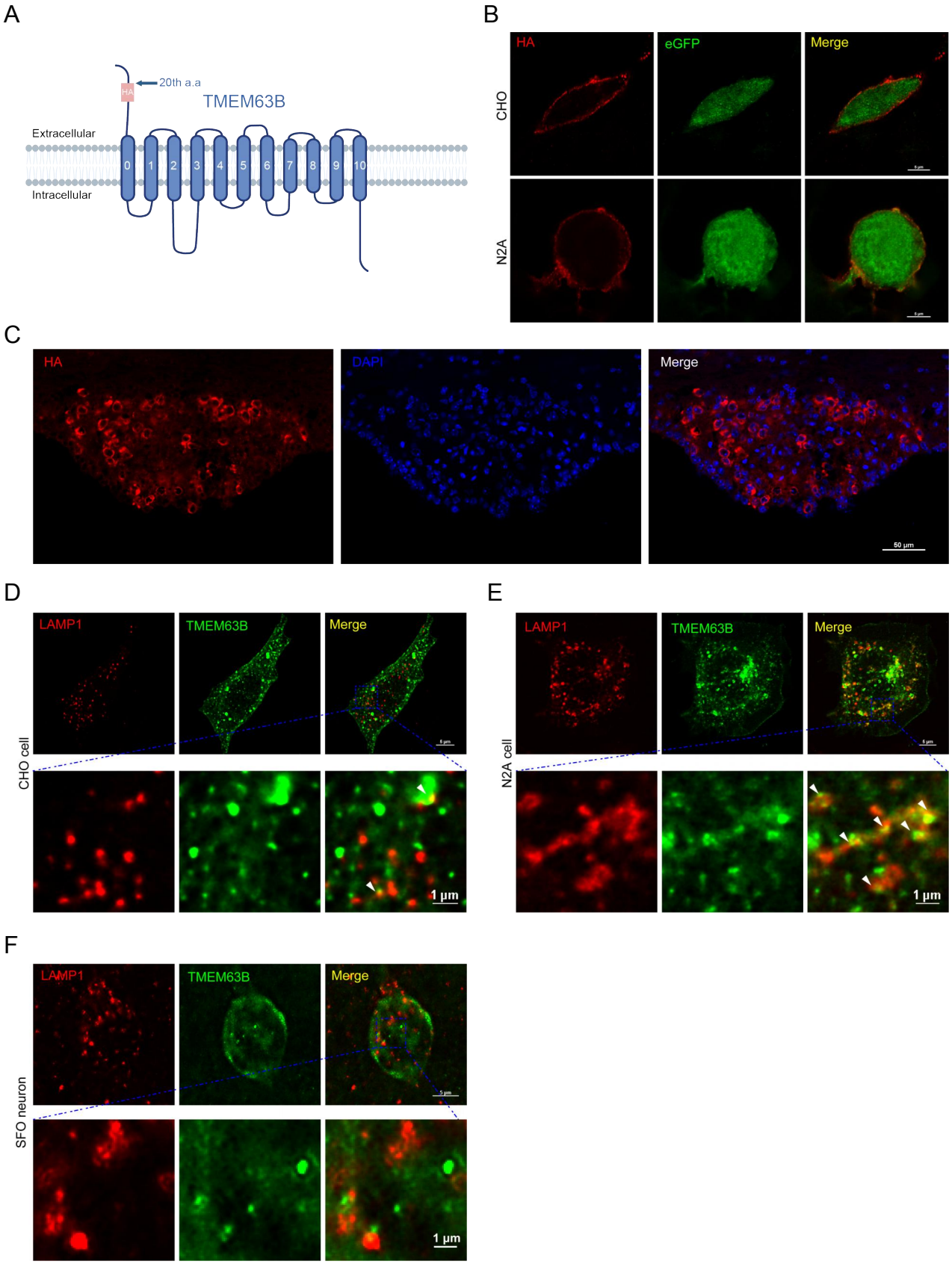
A
20th a.a
HA
TMEM63B
Extracellular
Intracellular
0
1
2
3
4
5
6
7
8
9
10
B
HA
eGFP
Merge
CHO
N2A
C
HA
DAPI
Merge
50 μm
D
LAMP1
TMEM63B
Merge
CHO cell
1 μm
E
LAMP1
TMEM63B
Merge
N2A cell
1 μm
F
LAMP1
TMEM63B
Merge
SFO neuron
1 μm

Figure S16. Subcellular localization of TMEM63B in CHO, N2A cells and SFO neurons, related to Figure 2.

(A) Schematic showing the position of extracellular N-terminal HA tag fused to TMEM63B proteins, which enables non-permeabilized staining.

(B) Non-permeabilized staining detecting the extracellular HA tag fused to heterologously expressed TMEM63B showed HsTMEM63B is widely distributed in plasma membrane of CHO and N2A cells. Non-fusion expressed eGFP (green), HA (red). Scale bar 5 μm.

(C) Non-permeabilized staining showed endogenous MmTMEM63B is widely distributed in plasma membrane of SFO neurons of *Tmem63b*$^{HA\text{-}fl/HA/fl}$ mice. Scale bar 50 μm.

(D) Heterologously expressed HsTMEM63B-eGFP is co-localization with a small fraction of endogenous LAMP1 in CHO cells.

(E) Heterologously expressed HsTMEM63B-eGFP is partially co-localization with endogenous LAMP1 in N2A cells.

(F) Endogenous MmTMEM63B in *Tmem63b*$^{HA\text{-}fl/HA/fl}$ mice is barely co-localization with LAMP1 in SFO neurons.

LAMP1 (red), TMEM63B is labeled by a fusion eGFP (green) for **(D)** and **(E)**. LAMP1 (red), TMEM63B is labeled by a fusion HA (green) for **(F).** Scale bar: top 5 μm, bottom 1 μm for **(D-F)**.

SUPPLEMENTAL REFERENCES

S1. Pool, A.H., Wang, T., Stafford, D.A., Chance, R.K., Lee, S., Ngai, J., and Oka, Y. (2020). The cellular basis of distinct thirst modalities. Nature *588*, 112-117. https://doi.org/10.1038/s41586-020-2821-8.